Noname manuscript No.
(will be inserted by the editor)

Mechanical behaviour in DC alloys casting processes

Patricia Barral · Peregrina Quintela · María Teresa Sánchez

Received: date / Accepted: date

Abstract The aim of this work is to give a review of algorithms computationally efficient to simulate the thermo-mechanical behaviour in casting processes; in particular, the butt curl deformation and the contraction of the lateral sides of the slab. The main aim is to give an overview of the most used methods to deal with the nonlinearities due to the thermo-elastic-viscoplastic laws of the involved materials and to the contact condition with the bottom block. To evaluate the efficiency of the proposed methods, some academic tests adapted to the difficulties arising in casting processes are presented. Applications of the techniques proposed to aluminium casting processes are discussed and numerical results are given.

Keywords Solidification processes · Thermal deformations · Maxwell Norton materials · Signorini contact condition · Duality methods · Bermúdez-Moreno algorithm · Newton methods · Finite element method

P. Barral
Department of Applied Mathematics, University of Santiago de Compostela
15782, Santiago de Compostela, SPAIN
Tel.: +34881813191
E-mail: patricia.barral@usc.es

P. Quintela
Department of Applied Mathematics, University of Santiago de Compostela
15782, Santiago de Compostela, SPAIN
Tel.: +34881813223
E-mail: peregrina.quintela@usc.es

M.T. Sánchez
Centro Universitario de la Defensa Zaragoza. Academia General Militar.
Ctra. de Huesca, s/n, 50090, Zaragoza, SPAIN
Tel.: +34976739808
E-mail: tererua@unizar.es

1 Introduction

The casting process is a manufacturing process that consists of pouring a liquid into a mould, which contains a hollow cavity of the desired shape, where it is allowed to solidify. The casting process of an alloy, composed of two or more metals, is a very complex and common process in industry. The predominant metal in the alloy is usually either aluminium, magnesium, zinc, copper, or, in some cases, lead or tin. There are a wide variety of casting processes in the industry depending on the concerned alloy, on the involved industrial application or on the required final geometry. Some of the most common processes are permanent mould casting, continuous casting, semicontinuous or direct chill casting, pressurized casting, die casting, lost foam casting, centrifugal casting, or sand casting.

Each casting process has its own features; however, there are phenomena that are common to all of them. The most common occurrences in casting processes having an adverse effect on process efficiency and hindering their optimization are:

- The contraction of the geometry or shrinkage due to the volumetric reduction that occurs in alloys during solidification.
- Cracking or tearing caused by thermal contraction stress that occurs just below the solidifying temperature.
- Fatigue processes that can be initiated by the large thermal gradients which appear during each casting cycle.
- The production of air or gasses from decomposition of release agents that can be encapsulated by the super heated liquid metal and being a source of porosity in the final slab.
- The formation of blow holes, voids or pores, which may occur due to entrapped gas or volumetric shrinkage during solidification.
- The formation of air-gaps between the die or mould and the slab, which has an adverse effect on process efficiency since it hinders the effective heat transfer, leading to longer solidification times.
- The degree of roughness of the surface of the produced casting piece which can require a strong final polishing.
- The formation of dendrites, that is, crystals with a branching tree like pattern.

A detailed description of casting processes can be found in Stefanescu [80]; this book discusses not only different developments in the field but also the applications of some fundamental sciences such as Physical Chemistry, Heat Transfer, or Fluid mechanics in alloys casting; it also includes a very large glossary of terms in this scope. In the literature there are many works dealing to a better understanding of one or more of the problems detailed above, in order to articulate new proposals in the casting design that avoid them, and to analyze the influence of the casting parameters in the solidifying piece (see Domitner *et al.* [36], Flemings [42], Kaufman and Rooy [54], Sołek and Trębacz [79] or Stoll [81]).

In this paper, the topic of computational modeling of thermo-mechanical behaviour in casting processes is reviewed; in particular, our aim is centered on a review of efficient algorithms to solve nonlinearities arising when modeling the mechanical stresses and deformations which occur during such processes. Here, we focus on the semi-continuous casting of aluminium alloys; nevertheless many of the proposed mathematical techniques are also applicable to other casting processes.

During semi-continuous casting of aluminium alloys, aluminium slabs are cast by pouring the metal through a water-cooled mould (DC casting) or an electromagnetic field (EMC casting) onto a shallow pan or bottom block. When the metal at the circumference of the slab cross-section has solidified, the bottom block starts moving downwards at the casting speed, leaving room for more liquid metal (see Figure 1). The exposed slab between the mould/electromagnetic field and the bottom block is cooled by jets of refrigerated water. A detailed description of the complete process can be found in Drezet and Plata [38] or Schneider *et al.* [78].

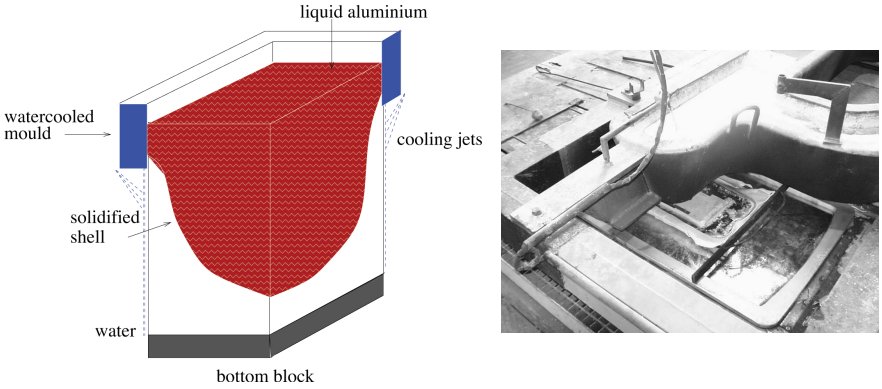

Fig. 1 Scheme of a DC casting process and a photograph of a mould (courtesy of ALCOA-INESPAL, A Coruña, Spain).

The whole semi-continuous casting process is very complex because there are many interconnected phenomena:

- Thermal phenomena with change of phase due to aluminium solidification, with strong thermal gradients within the slab and very abrupt changes of temperature in small time intervals. Due to the large thermal stresses inside the slab, the butt curls and then the heat transfer between the slab and the bottom block changes (see Kim [56]).
- Mechanical phenomena promoted by the large thermal stresses developed inside the slabs and by the solidification shrinkage due to the easy deformability of the recently solidified aluminium in the mould.
- Electromagnetic phenomena due to an alternating current traveling the inductor which produces the electromagnetic forces to confine the metal in EMC casting.

- Hydrodynamic phenomena in the liquid phase due to the Lorentz forces (for the EMC casting) and to natural convection coming from the temperature gradients.
- Free boundary phenomena: the meniscus is shaped when the liquid metal is confined (for the EMC casting), whereas the knowledge of the solid-liquid interface plays a major role in the casting process.
- Physical chemistry phenomena: during solidification of metallic alloys, a continuous transition from the liquid to the solid state takes place. Below the liquidus temperature and due to local under cooling, nucleation of solid germs happens; in this first stage, at small solid fractions, the solid germs grow independently and the solid dendrites are completely free to move. After a further temperature decrease, the dendrites contact each other and begin to agglomerate.

A description of the mathematical involved models is given, for instance, in Barral et al. [4], where several models are proposed describing some thermal, mechanical, electromagnetic and hydrodinamical phenomena arising from the EMC casting process; in El-Raghi *et al.* [40] or Otero [70] for thermal submodel; in Agelet de Saracibar *et al.* [1] for the coupled thermo-mechanical model or in Bermúdez and Muñiz [20] or Bermúdez *et al.* [21] for hydrodynamical and electromagnetic one.

Numerical simulation of casting processes has aroused great interest in the last forty years. In recent years, the decreasing of computational costs and the increasing power of commercial modelling packages have facilitated the application of mathematical models and their numerical simulation as an additional tool to understand complex industrial processes such as casting processes.

Numerical simulation of the behaviour of the DC casting process is being extensively used to improve the design of new casters and to analyze the influence of the casting parameters in the solidifying slab, namely, casting speed, slab size, mould shape, casting temperature, flow rate of cooling water and so on. Numerical simulation of such problems has already been considered by several authors but in almost all cases without clear explanation of the algorithms that might be used to solve the proposed models (see Besson *et al.* [25], Drezet *et al.* [37], El-Raghy *et al.* [40], Hongjun *et al.* [53], Le *et al.* [59], Mariaux *et al.* [64], Subroto *et al.* [82] or Xu *et al.* [88] and the references therein). Furthermore, the staggering complexity of this process makes almost impossible to model all the phenomena mentioned above together at once, so the various numerical submodels reported in the literature are not yet fully coupled and the large-scale numerical simulation of these processes continues to be nowadays a very complex task.

In this paper we restrict ourselves to the modelling and numerical simulation of the thermo-mechanical phenomena which appear in the aluminium DC casting. Thus, we assume that the temperature field is calculated prior to thermo-mechanical deformation. The only relationship between the thermal and the mechanical models we have considered is that the heat transfer coeffi-

cient between the slab and the bottom block surface depends on time, surface temperature and the intrusion of cooling water into the gap created by the butt curl. The thermal model to predict temperature of the solidifying slab corresponds to a transient heat conduction equation where latent heat evolution and heat capacity are incorporated into the constitutive equation; these data must be also supplied to relate temperature with enthalpy. In Barral *et al.* [4], Bermúdez *et al.* [23] and Otero [70], appropriate boundary conditions are provided to define heat input to every portion of the slab boundary. For a complete description of the thermal submodel see also Ciavaldini [34] or El-Raghy *et al.* [40].

From a thermo-mechanical point of view, DC casting process can be divided into two stages:

- The *start stage*, during which the temperature field, the solidification front, and the slab shape change with time. During this phase, due to the large thermal stresses, the butt of the slab curls and loses contact with the bottom block (see Figure 2). This deformation, known as butt curl, takes place when the direct water cooling hits the slab surface. The air gap left by the butt curl may reach the height of approximately 100mm, depending on the slab size and the casting conditions. The butt curl could induce instability of the slab, the formation of cracks and therefore the breakthrough of liquid metal, so, in the worst case, could lead to the interruption of the casting.
- The *stationary stage*. When the length of the slab is 1m, approximately, the temperature field has attained a steady state. In this stationary stage, the hot exterior of each aluminium slab attempts to expand but it is constrained by its colder interior and the cold water stiff mould; this makes each plate bend in toward the solidifying aluminium. This phenomenon is known as solid shrinkage and it is critical for two important reasons: First, the shrinkage must be predicted and then built into the moulds dimensions. If this is not correctly done, then the tooling will need to be modified iteratively to achieve an acceptable production casting. This adds time and cost to the design cycle and introduces quality risk in the final product. To compensate the shrinkage effects, if the desired final shapes have rectangular section, the designed mould shapes are convex, usually with three segments (see Figure 3). Second, as the casting cools, it may not be able to shrink uniformly because some regions are stiffer than others. This can result in undesirable residual stresses and/or undesirable warpage (see Stoll [81]). Creating geometries that make shrinkage predictable and that avoid residual stresses and warping is therefore highly desirable.

To predict casting thermo-mechanical behaviour, the main difficulties are due to the previously mentioned coupling effects –at each time instant, the mechanical parameters depend on temperature–, to the presence of nonlinear terms –mechanical behaviour law of the alloys at high temperatures, the unilateral contact between the slab and the bottom block–, to the existence of free boundaries –the solid liquid interface, where the weight of the liquid should be

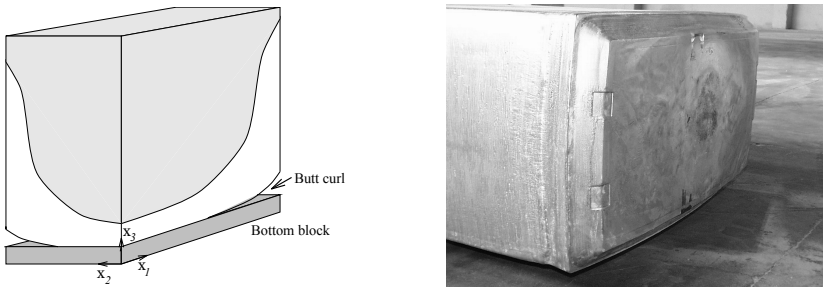

Fig. 2 Scheme of the butt curl deformation and a photograph of the resulting slab (courtesy of ALCOA-INESPAL, A Coruña, Spain)

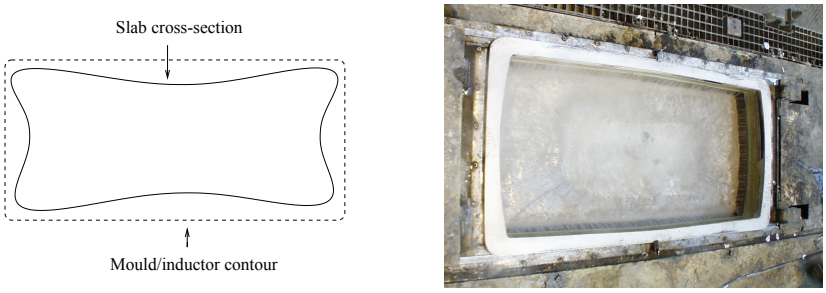

Fig. 3 Scheme of the lateral faces contraction due to solid shrinkage and a photograph of the mould (courtesy of ALCOA-INESPAL, A Coruña, Spain)

considered as a load on the solidified part– and to the growth of the computational domain with time at casting speed (see [4]). Specifically, in order to simulate the butt curl deformation of aluminium casting processes, we must solve a problem of frictionless unilateral contact between a thermo-elastic-viscoplastic body, with mechanical coefficients strongly dependent on the temperature, and a rigid foundation. This problem is posed on a computational domain corresponding to the portion of the solidified slab, which is a domain obtained from the solution of the corresponding thermal submodel at each time instant. In particular, following the works of Drezet *et al.* [37], Kristiansson and Zetterlund [58] and Mariaux *et al.* [64], we assume that the alloy is a Maxwell-Norton elastic-viscoplastic material, which is a behaviour law frequently used in alloy solidification processes. This law was deeply studied from a mathematical point of view in Blanchard and Le Tallec [26], Djaoua and Suquet [35], Friaâ [44], Geymonat and Suquet [46], Le Tallec [60] or Teman [84].

This manuscript is not only a joint presentation of research conducted by the authoresses in this area (see [3–15]) but also a review of the related literature. In particular, several mathematical and numerical aspects of this subject are presented:

– The detailed formulation as a variational inequality. It correspons to a quasi-static evolution problem for a three-dimensional, elastic-viscoplastic

solid obeying a Signorini contact condition with the bottom block (see [7, 8]).

- The establishment of sufficient conditions for the existence of a solution. For this purpose, we have adapted the techniques developed by Djaoua and Suquet [35] for viscoelastic problems with mixed boundary conditions to also include Signorini conditions.
- The numerical implementation of the metallostatic pressure on the liquidus-solidus interphase. One of the main difficulties in the numerical solution of this problem is the right imposition of the metallostatic pressure exerted by the liquid metal on the recently solidified one, that is, on the upper boundary of the computational domain, which is the isotherm corresponding to the liquidus temperature and so the free boundary of the associated thermal problem. For that purpose, following Hannart *et al.* [50], we have proposed a fictitious domain method: we have modelled the entire slab, replacing the liquid metal by a very weak elastic material under the action of gravity forces, which therefore does not offer resistance to solid deformations. This methodology has the advantage that remeshing to adjust the free boundary is not needed at each time step, and so the numerical implementation is easier. Nevertheless, numerical simulations showed that it was not sufficient to consider a very weak elastic law in the fictitious domain since the solution was strongly dependent on the Lamé coefficients. In fact, using an asymptotic technique, it was proved that only a proper relationship between the fictitious Lamé coefficients leads to a correct laying of the metallostatic pressure on the thermal free boundary (see [10,11]).
- The numerical approximation of the variational inequality and the description of a standard numerical scheme to solve it. An approximate solution of this problem was obtained by using an implicit Euler scheme in time and a finite element method in space (see [3]). To deal with the nonlinearities, the numerical solution was based on the Bermúdez-Moreno algorithm with the participation of two multipliers: a viscoplastic multiplier –to take into account the nonlinearity from the behaviour law– and a contact multiplier –to avoid the nonlinearity due to the contact condition– (see [7,8] or Bermúdez and Moreno [19]). Each of these multipliers is the fixed point of a nonlinear equation; their numerical computation using a classical fixed point method constitutes the Standard Bermúdez Moreno algorithm (SBM algorithm).

  In DC casting process, numerical computation of contact or viscoplastic multipliers using SBM algorithm presents several difficulties related with the strong nonlinearity of the behaviour law in the regions close to the recently solidified material (see [8]). Indeed, during the stationary stage, in which the contact condition does not have a significant influence, SBM algorithm works well; however, during the start stage, when two nonlinearities appear together, the convergence is worse, increasing considerably the cpu-time. Moreover, SBM algorithm presents a strong dependence on its parameters, which can not be determined *a priori*. These facts made difficult the massive usage of this algorithm to help in the understanding

of the different effects in casting processes. That is why we have tried to develop efficient numerical methods that incorporate adaptive procedures to accelerate the treatment of the nonlinearities and hence, to be able to simulate the butt curl deformation in a reasonable cpu-time.

- Improvements in the treatment of the contact condition. We propose to approximate the contact multiplier with a generalized Newton method together with a penalization technique to conserve the matrix's symmetry (see [5,15], Glowinski and Le Tallec [47], Kikuchi and Oden [55] or Robinson [75]). The resultant algorithm for the treatment of the contact condition is fast, accurate and its convergence is independent of the algorithm parameters. Nevertheless, the stiffness matrix needs to be recalculated at each iteration. Furthermore, the stiffness matrix has a high condition number due to the different scale of the material parameters –fictitious/solid–; due to this, iterative solvers have convergence problems when they are applied to solve the discretized system. So, taking into account that usually the nonlinear boundary condition only involves a small part of the boundary that is time independent, we propose to use a direct method combined with a partial factorization of the stiffness matrix adapted to the problem's geometry.
- Improvements in the treatment of viscoplastic law. Two options are considered:
  - Approximating the viscoplastic multiplier with standard Newton techniques without modification of the stiffness matrix at each iteration (see [5,15]). When there are strong thermal gradients, it becomes necessary to employ some numerical strategies to obtain a good convergence of the viscoplastic multiplier: an adimensionalization technique, an Armijo rule and an automatic optimization of the time step. We present academic tests in order to show the good behaviour of this methodology. Nevertheless, in real casting processes, the convergence is not always achieved with it.
  - Approximating the viscoplastic multiplier with a generalization of the SBM algorithm with variable parameters which are automatically computed (see [14], Gallardo *et al.* [45] or Parés *et al.* [74]). This procedure does not present the convergence problems in the regions close to the solidification front that the two previous algorithms have, and it could be also applied to other solidification problems with a strong dependence on the temperature gradients.

Summing up, the outline of this paper is as follows. In Section 2, we will show a detailed description of the mathematical model corresponding to the thermo-mechanical behaviour of a DC casting of aluminium alloy; it is a quasistatic model posed on the already solidified part of the slab and whose boundary conditions include a contact condition of Signorini type. A carefully presentation of the behaviour law of the alloy will be given in Subsection 2.2.3. In Section 3 we will summarize the main assumptions on the data and the functional framework to obtain a standard weak formulation of the thermo-

mechanical problem as a variational inequality formulated on the solidified slab. The main results concerning the mathematical analysis of a simplified submodel will also be given in Section 3.3. Section 3.4 will be devoted to justify a fictitious domain technique to impose the metallostatic pressure exerted by the liquid metal; with this methodology, the liquid is replaced by a fictitious material and a new weak formulation on the entire slab is introduced in Subsection 3.4.2. This latter weak problem will be discretized in time by an implicit Euler scheme and in space by means of a finite element method in Section 4. Following the maximal monotone operator techniques, we will propose three iterative algorithms to solve the discretized problem: the Standard Bermúdez Moreno algorithm (SBM algorithm) in Section 4.2; its improvement with Newton methods to approach the contact and viscoplastic multipliers (NBM algorithm) in Section 4.3; and in Section 4.4 we will present a combination of a Newton method to approach the contact multiplier with the SBM algorithm improved with an automatic computation of the parameters involved in the approach of the viscoplastic multiplier (VNBM algorithm). Along this section we will include several academic tests to analyze the efficiency of each of the presented algorithms. In Section 5, we will present some numerical results obtained for a real casting process with the three proposed algorithms.

2 Mathematical model

In this section we introduce a mathematical model to simulate the thermo-mechanical deformations suffered by an aluminium slab during the solidification process. Several authors analyzed the mechanical deformations in this type of processes. In 1982, Kristiansson and Zetterlund [58] studied the deformation in a steel continuous casting by means of a two-dimensional viscoelastic model, formulated on a horizontal section. Later, in 1992, Mariaux *et al.* [64] studied the butt curl simulation in aluminium castings and, in 1995, Drezet *et al.* [37] simulated their cross-sectional deformation; both works considered a behaviour law of Maxwell-Norton type. In 1999, Cervera *et al.* [30] presented a fully coupled thermo-mechanical problem for numerical simulation of solidification processes of industrial metal parts; in that paper, mechanical and thermal properties were assumed to be temperature-dependent whereas the evolution of the plastic strains was defined in the usual way for a J2-thermo-elastic-viscoplastic model. More recently, Bellet *et al.* [16] presented a model of pipe formation in metal castings in which a viscoplastic law with hardening for the solid was proposed. In this work, we consider the thermo-elastic-viscoplastic law of Maxwell-Norton type used in Drezet *et al.* [37] and Mariaux *et al.* [64], and already studied by the authoresses in [8]. Special attention has been paid to the modelling of the behaviour law in this section. In particular, in Subsection 2.2.3, a thermal law whose coefficient of thermal expansion includes the volume changes due to possible phase shifts is presented; and also a complete analysis of the viscoplastic law, modelling the secondary creep, which incorporates the temperature dependence in the strain rate tensor.

As we have announced in the introduction, in this work coupling between thermal and mechanical models is not considered and, therefore, the temperature field is computed *a priori* and introduced as a data in the mechanical simulation. Nevertheless, to ease the reading of this paper, in Section 2.1 we briefly describe the mathematical model used to compute the temperature field; further information about this model can be found in Barral *et al.* [4] and Bermúdez and Otero [23]. Next, in Section 2.2 we present a mathematical model to compute the thermo-mechanical deformation, deeply studied in [4, 5,7,8,14].

Hereafter in this paper, Latin subscripts are understood to range over the integers $\{1,2,3\}$, and Greek subscripts over the integers $\{1,2\}$. Einstein notation of summation over repeated subscripts is implied.

2.1 Mathematical model of the thermal problem

In this section, we introduce the mathematical model with phase change to calculate the temperatures studied by Bermúdez and Otero (see [4,23,70]), and used as a data in the mechanical model.

Thermal models for alloys solidification can be included in the family of the two-phase Stefan problems (see for instance Meirmanov [66] or Rubinstein [76]). During solidification processes, there exists an interphase which separates the solid and liquid parts. The classical heat equation is verified at both sides of the interphase, but in the interphase a loss of latent heat of fusion is produced. In order to solve this Stefan problem there exist two different options: front tracking and fixed domain methods (see details in Lewis and Ravindran [62] and references therein). In front tracking methods the solid and liquid phases are treated as two separated domains for which it is necessary to follow the interphase and to remesh at each time step of the discretization (see Sullivan and Lynch [83] and Yoo and Rubinsky [89,90]). Contrarily, fixed domain methods treat both regions as one continuous domain, defining the interphase in an implicit way by means of an auxiliary variable, so remeshing is not necessary. The most employed fixed domain methods in casting modeling are enthalpy and effective specific heat methods. The first type rewrites the heat conduction equation in terms of the enthalpy, which implicitly includes the latent heat (see Casella and Giangi [29], Durany [39] and Nedjar [69]), whereas the second one introduces a fictitious specific heat to take it into account (see Drezet *et al.* [37] and El-Raghy *et al.* [40]). For instance, the thermal problem for continuous casting was solved by using the entalphy method in Chen and Jiang [31], Chen *et al.* [32] or Wu *et al.* [87]; and by Barral *et al.* [4] and Bermúdez and Otero [23] for DC casting.

In this paper, following the latter two references, we use the temperature field computed from an enthalpy formulation. For the sake of simplicity, convective heat transfer in the liquid phase is neglected. The thermal problem including this term was studied by Bermúdez and Otero [23,70] to take into account the effect of the fluid movement.

Let $Ox_1x_2x_3$ be a fixed system of rectangular Cartesian axes associated to the slab and $[0, t_f]$ be the time interval to carry out the thermo-mechanical simulation. Due to casting symmetry, $\Omega(t) \subset \mathbb{R}^3$ represents a quarter of the slab at the time instant $t \in [0, t_f]$ and $\Omega(0)$ represents the aluminium inside the bottom block when it begins to go down. Notice that the mould and bottom block are not part of the thermo-mechanical domain. We model the going down of the bottom block with an upward displacement of the mould. Figure 4 shows the computational domain $\Omega(t)$ and a scheme of the behaviour of the casting process in a vertical section.

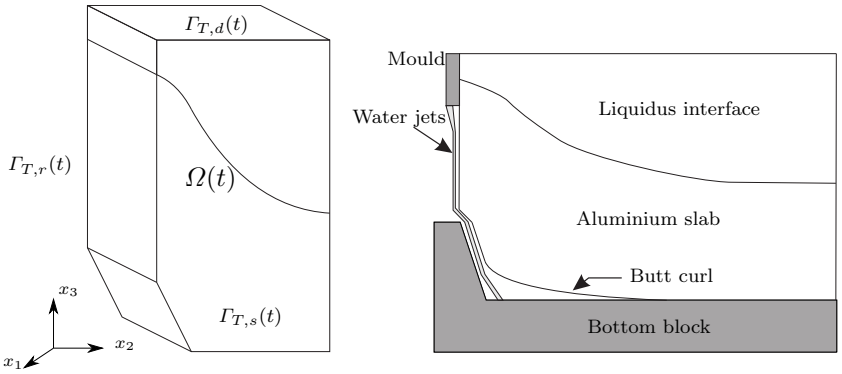

Fig. 4 Computational domain of the thermal problem, $\Omega(t)$, and scheme of a vertical section of a DC casting process.

The thermal problem consists of determining the temperature field $T(\mathbf{x}, t)$ at each point $\mathbf{x} \in \Omega(t)$ and at each $t \in (0, t_f]$.

Let T_s, T_l be the solidus and liquidus temperature, respectively. Alloy solidification occurs at the temperature range $[T_s, T_l]$, $T_s < T_l$, since each alloy component holds a different solidus temperature, appearing a mushy region in this temperature interval. For these non isothermal processes, the enthalpy function is defined by

$$H(T) = \begin{cases} \displaystyle\int_0^T \rho(s)c(s)ds & \text{if } T < T_s, \\ \displaystyle\int_0^T \rho(s)c(s)ds + \frac{L}{T_l - T_s}\int_{T_s}^T \rho(s)ds & \text{if } T_s \le T \le T_l, \\ \displaystyle\int_0^T \rho(s)c(s)ds + \frac{L}{T_l - T_s}\int_{T_s}^{T_l} \rho(s)ds & \text{if } T > T_l, \end{cases} \tag{1}$$

where L is the latent heat per unit mass, $\rho(T)$ the mass density per unit volume and $c(T)$ the specific heat of the material per unit mass; both ρ and c are assumed to be dependent on temperature.

Notice that when the phase change occurs at a fixed temperature, that is, $T_s = T_l$, the enthalpy $H(T)$ is the following multivalued function:

$$H(T) = \begin{cases} \displaystyle\int_0^T \rho(s)c(s)ds & \text{if } T < T_s, \\ \displaystyle\left[\int_0^{T_s} \rho(s)c(s)ds, \int_0^{T_s} \rho(s)c(s)ds + \rho_s L\right] & \text{if } T = T_s, \\ \displaystyle\int_0^T \rho(s)c(s)ds + \rho_s L & \text{if } T > T_s, \end{cases}$$

where $\rho_s = \rho(T_s)$ is the density at solidus temperature (see Otero [70] for details). These isothermal solidification processes occur, for example, in pure metals.

Assuming that there is no internal heat source, the heat conduction equation remains:

$$\frac{\partial H(T)}{\partial t} - \mathrm{Div}(k_T(T)\nabla T) = 0 \text{ in } \Omega(t), \forall t \in (0, t_f), \tag{2}$$

where k_T is the thermal conductivity of the material.

Next, let $\Gamma_T(t)$ be the boundary of $\Omega(t)$ and $\mathbf{n}$ the unit outward vector, normal to $\Omega(t)$. Boundary $\Gamma_T(t)$ is decomposed into three disjoint and open parts as follows (see Figure 4):

$$\Gamma_T(t) = \bar{\Gamma}_{T,r}(t) \cup \bar{\Gamma}_{T,s}(t) \cup \bar{\Gamma}_{T,d}(t),$$

where:

- $\Gamma_{T,r}(t)$ denotes the lateral outer and lower faces of the slab which are in contact with air, water or the bottom block. On this boundary, the heat transfer is produced by convection, so

$$k_T(T)\frac{\partial T}{\partial \mathbf{n}} = \alpha_T(T_e - T) \text{ on } \Gamma_{T,r}(t),$$

  where $\alpha_T(\mathbf{x}, t)$ is the convection heat transfer coefficient and $T_e(\mathbf{x}, t)$ the temperature of surroundings.
- $\Gamma_{T,d}(t)$ is the upper boundary of $\Omega(t)$; here, the temperature, which corresponds with the casting one, is known and it is denoted by T_d. In this boundary, we impose the Dirichlet condition

$$T(\mathbf{x}, t) = T_d(\mathbf{x}, t) \text{ on } \Gamma_{T,d}(t).$$

- $\Gamma_{T,s}(t)$ are the symmetry boundaries, where we impose the usual symmetry condition

$$k_T(T)\frac{\partial T}{\partial \mathbf{n}} = 0 \text{ on } \Gamma_{T,s}(t).$$

Finally, we introduce the initial condition

$$T(\mathbf{x}, 0) = T_0(\mathbf{x}) \text{ in } \Omega(0),$$

where T_0 is the temperature distribution in $\Omega(0)$.

Summing up, the thermal problem to solve is the following:

Problem (TP):
Find the temperature field $T(\mathbf{x}, t)$ at each point $\mathbf{x} \in \Omega(t)$ and at each instant $t \in (0, t_f]$ such that:

$$\frac{\partial H(T)}{\partial t} - \text{Div}(k_T(T)\nabla T) = 0 \quad \text{in} \quad \Omega(t), \tag{3}$$

$$k_T(T)\frac{\partial T}{\partial \mathbf{n}} = \alpha_T(T_e - T) \quad \text{on} \quad \Gamma_{T,r}(t), \tag{4}$$

$$k_T(T)\frac{\partial T}{\partial \mathbf{n}} = 0 \quad \text{on} \quad \Gamma_{T,s}(t), \tag{5}$$

$$T = T_d \quad \text{on} \quad \Gamma_{T,d}(t), \tag{6}$$

$$T(0) = T_0 \quad \text{in} \quad \Omega(0), \tag{7}$$

where $H = H(T)$ is defined by expression (1).

In Barral *et al.* [4], the following numerical procedure to solve Problem (TP) is proposed:

- Firstly, in order to overcome the nonlinearity due to the diffusion term in the heat equation, the Kirchhoff transformation is introduced (see also Özisik [71]).
- The resulting equations are discretized using an implicit Euler method in time and a finite element method in space.
- The free boundary given by the solidification front is handled by using a fixed domain method.

Numerical results for the real casting thermal simulations showing the accuracy of this method and a good agreement with experimental measurements of the physical problem can be also seen in Barral *et al.* [4]. This methodology is used in this work to compute the temperatures necessary to determine the thermo-mechanical deformation.

2.2 Mathematical model of the thermo-mechanical problem

The mechanical domain at each time instant $t \in [t_0, t_f]$ corresponds to the solidified part of a quarter of the slab, $\Omega_s(t)$, which is obtained from the solution of the thermal problem (TP) (see Figure 5):

$$\Omega_s(t) = \{\mathbf{x} \in \Omega(t); T(\mathbf{x}, t) < T_l\}.$$

Notice that the initial time in the mechanical simulation is $t_0 > 0$ in order to ensure that the initial solidified part of the slab is nonempty, $\Omega_s(t_0) \neq \emptyset$.

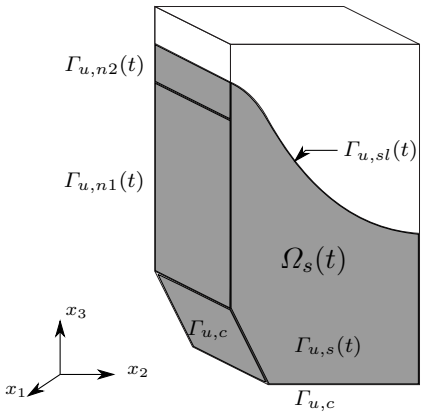

Fig. 5 Mechanical domain $\Omega_s(t)$ (shading part).

The mechanical problem consists of determining the displacement field $\mathbf{u}(\mathbf{x},t)$ and the stress tensor field $\boldsymbol{\sigma}(\mathbf{x},t)$ at each point $\mathbf{x} \in \Omega_s(t)$ and at each time instant $t \in (t_0, t_f]$.

2.2.1 Equilibrium equation

Under the small strains assumption and in the quasistatic case, the slab behaviour is governed by the equilibrium equation

$$-\mathrm{Div}(\boldsymbol{\sigma}) = \mathbf{f} \text{ in } \Omega_s(t),$$

where $\mathbf{f}$ represents the volume forces due to the gravity, that is,

$$\mathbf{f}(\mathbf{x},t) = (0, 0, -\rho(T(\mathbf{x},t))g)\,.$$

2.2.2 Boundary conditions

In the mechanical simulation, the boundary $\Gamma_u(t)$ of the solidified slab $\Omega_s(t)$ is split into five disjoint and open parts (see Figure 5):

$$\Gamma_u(t) = \bar{\Gamma}_{u,sl}(t) \cup \bar{\Gamma}_{u,c} \cup \bar{\Gamma}_{u,s}(t) \cup \bar{\Gamma}_{u,n1}(t) \cup \bar{\Gamma}_{u,n2}(t),$$

where:

- the upper boundary $\Gamma_{u,sl}(t)$ is defined by the isotherm corresponding to the liquidus temperature T_l;
- $\Gamma_{u,c}$ is the part of the slab susceptible to be in contact with the bottom block;
- $\Gamma_{u,n1}(t)$ denotes the part of the lateral outer faces which has already solidified and therefore it is free of forces;
- $\Gamma_{u,n2}(t)$ corresponds to the outer boundary of the mushy region, which is confined by the mould;
- and finally, $\Gamma_{u,s}(t)$ denotes the symmetry boundary, where we assume usual symmetry conditions.

Metallostatic pressure. On boundary $\Gamma_{u,sl}(t)$ we impose the metallostatic pressure exerted by the overlying liquid metal

$$\boldsymbol{\sigma}\mathbf{n} = p_r\mathbf{n},\ p_r(\mathbf{x},t) = \rho_l\, g(x_3 - h(t)) \text{ on } \Gamma_{u,sl}(t),\ t_0 < t \leq t_f,$$

where $\rho_l = \rho(T_l)$ is the density at liquidus temperature and $h(t)$ is the length of the slab at the instant t. Notice that, since $\Gamma_{u,sl}(t)$ is the thermal free boundary, it varies with time and it is a data for the mechanical problem.

Contact condition. The bottom block is assumed to be rigid, so aluminium cannot penetrate it; that means that the normal component of displacements, $u_n = \mathbf{u}\cdot\mathbf{n}$, cannot be positive:

$$u_n \leq 0 \text{ on } \Gamma_{u,c}\times(t_0,t_f].$$

Moreover, due to the action-reaction principle, where an effective contact exists, the bottom block exerts an upwards pressure in the normal direction. Consequently, if $u_n = 0$, the normal stress, $\sigma_n = \boldsymbol{\sigma}\mathbf{n}\cdot\mathbf{n}$, verifies $\sigma_n \leq 0$. Contrarily, where a contact does not exist, the distance between the slab and the bottom block is not null and, consequently, the motion is unconstrained; so, if $u_n < 0$, then $\sigma_n = 0$. Finally, taking into account that water is flowing down on the slab sides, we assume that friction is not significant in the contact zone; so, we suppose that the tangential stresses, called shear stresses, $\boldsymbol{\sigma}_t = \boldsymbol{\sigma}\mathbf{n} - \sigma_n\mathbf{n}$, are null.

Summing up, to reproduce the butt curl deformation, we consider the following frictionless contact condition with the bottom block

$$\boldsymbol{\sigma}_t = \mathbf{0},\ \sigma_n \leq 0,\ u_n \leq 0,\ \sigma_n u_n = 0 \text{ on } \Gamma_{u,c}\times(t_0,t_f].$$

This contact condition is known as *Signorini unilateral frictionless contact condition*. A detailed description can be found in Kikuchi and Oden [55] or Wriggers [86].

2.2.3 Behaviour law

We assume that the alloy is a nonlinear thermo-elastic-viscoplastic solid; so, the strain rate tensor is the superposition of elastic, thermal and viscoplastic components:

$$\boldsymbol{\varepsilon}(\dot{\mathbf{u}}) = \dot{\boldsymbol{\varepsilon}}^{\mathrm{e}} + \dot{\boldsymbol{\varepsilon}}^{\mathrm{th}} + \dot{\boldsymbol{\varepsilon}}^{\mathrm{p}}, \tag{8}$$

where the upper dot denotes the usual time derivative and the strain tensor is related to the displacement field by the usual formula

$$\varepsilon_{ij}(\mathbf{u}) = \frac{1}{2}(\partial_j u_i + \partial_i u_j).$$

Elastic behaviour law. The elastic deformations $\boldsymbol{\varepsilon}^e$ are related to the stress tensor $\boldsymbol{\sigma}$ through a Hooke's law with material parameters depending on temperature

$$\boldsymbol{\varepsilon}^{\mathrm{e}} = \Lambda(T)\boldsymbol{\sigma} = \frac{1+\nu(T)}{E(T)}\boldsymbol{\sigma} - \frac{\nu(T)}{E(T)}\mathrm{tr}(\boldsymbol{\sigma})\mathbf{I}, \tag{9}$$

where E, ν denote the Young's modulus and Poisson's ratio, respectively, and $\mathbf{I}$ is the identity tensor. Reciprocally, for this law the stress tensor $\boldsymbol{\sigma}$ can be written in terms of the strain tensor $\boldsymbol{\varepsilon}^e$,

$$\boldsymbol{\sigma} = (\Lambda(T))^{-1}\,\boldsymbol{\varepsilon}^e = \lambda(T)\mathrm{tr}(\boldsymbol{\varepsilon}^e)\mathbf{I} + 2\mu(T)\boldsymbol{\varepsilon}^e,$$

where λ and μ denote the Lamé coefficients, which are related with E and ν by the usual expressions:

$$\lambda(T) = \frac{E(T)\nu(T)}{(1+\nu(T))(1-2\nu(T))},\ \mu(T) = \frac{E(T)}{2(1+\nu(T))}.$$

This law is also applied to solidification processes in Cervera *et al.* [30]. A detailed description of Hooke's law can be found in Ciarlet [33], Gurtin [48], Gurtin *et al.* [49] or Marsden and Hughes [65].

Thermal law. The thermal expansion is related to the temperature by a generalized Arrhenius law

$$\dot{\boldsymbol{\varepsilon}}^{\mathrm{th}} = \alpha(T)\dot{T}\mathbf{I}, \tag{10}$$

where α is the coefficient of thermal expansion, including volume changes due to possible phase transformations. We use the following expression for α deduced in [3]:

$$\alpha(T) = -\frac{1}{3}\frac{\rho_l^{1/3}}{\rho(T)^{4/3}}\frac{d\rho(T)}{dT}. \tag{11}$$

This law generalizes other laws that can be found in the bibliography. For example, in Mariaux *et al.* [64] the thermal strain is described via an effective thermal dilatation coefficient, defined by

$$\alpha_{ls} = \frac{\rho_s - \rho_l}{3\rho_l(T_l - T_s)}.$$

Notice that this is an approximation of $\alpha(T_l)$ if we consider

$$\frac{d\rho(T)}{dT}|_{T=T_l} \approx \frac{\rho_l - \rho_s}{T_l - T_s}.$$

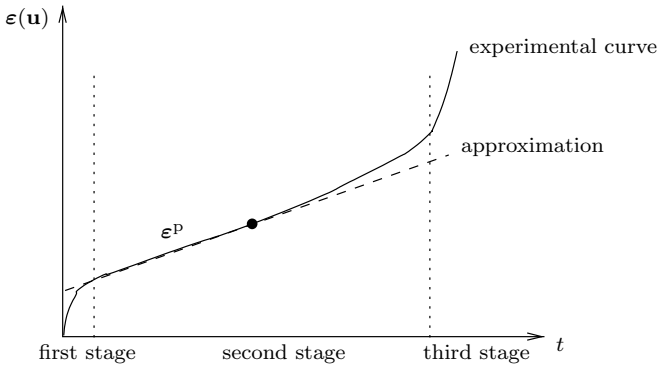

Fig. 6 Experimental creep curve.

Viscoplastic behaviour law. When a metal alloy is subjected to an increase of stresses, three stages can be observed:

- For small stresses the solid responds elastically; this means that the stress is proportional to the strain and the deformation is reversible.
- If the stress exceeds a critical magnitude, the behaviour ceases to be linear and the strain rate is nearly constant; this phenomenon is known as creep.
- In the third stage, the strain rate increases before fracture.

In particular, for a creep test at constant temperature, where the stresses are assumed to be constant in time, the second stage is quickly attained (see Figure 6). In order to model the two first stages, we approach the rate strain by a straight line, tangent to the inflection point of the curve (see Figure 6). In this work we do not consider the third stage and so fracture mechanisms are not taken into account.

To describe the effects of the secondary creep in the three-dimensional case, we use the classical Norton-Hoff law (see Friaâ [44] or Lemaitre and Chaboche [61]). This law was introduced by Norton in 1929 to model the unidimensional creep for steel at high temperature. Afterwards, in 1954, it was generalized to the multidimensional case by Hoff and the resultant law is known as Norton-Hoff law. This law depends on a material parameter q; in the limit case, when q goes to infinity, Friaâ [43,44] proved that it coincides with the Von Mises law of perfect plasticity. Furthermore, in Friaâ [44] new generalizations of the Norton law to the multidimensional case, known as generalized Norton-Hoff laws, were proposed.

Let us introduce the Von Mises convex

$$K = \{\boldsymbol{\tau} \in \mathcal{S}_3;\ |\boldsymbol{\tau}^D| \leq \sqrt{2}k\}, \tag{12}$$

where $\mathcal{S}_3$ is the space of symmetric second order tensors, $\boldsymbol{\tau}^D$ denotes the deviatoric tensor, defined by

$$\boldsymbol{\tau}^D = \boldsymbol{\tau} - \frac{1}{3}\mathrm{tr}(\boldsymbol{\tau})\mathbf{I},\ \boldsymbol{\tau} \in \mathcal{S}_3,$$

and k is a constant which represents the elastic limit in simple shearing (see Hill [52]). Let I_K denote the indicator function of convex K,

$$I_K(\boldsymbol{\tau}) = \begin{cases} 0 & \text{if } \boldsymbol{\tau} \in K, \\ +\infty & \text{in another case.} \end{cases}$$

Following Le Tallec [60] and Teman [84], we introduce its polar function as

$$I_K^*(\boldsymbol{\tau}) = \sup_{\boldsymbol{\xi} \in K} \{\boldsymbol{\tau} : \boldsymbol{\xi}\} = \begin{cases} \sqrt{2}k|\boldsymbol{\tau}| \text{ if } \mathrm{tr}(\boldsymbol{\tau}) = 0, \\ +\infty \quad \text{in another case.} \end{cases}$$

Let $\theta(\boldsymbol{\tau})$ be the calibrator function of K

$$\theta(\boldsymbol{\tau}) = \inf\{s; \boldsymbol{\tau} \in sK, s > 0\} = \frac{|\boldsymbol{\tau}^D|}{\sqrt{2}k}. \tag{13}$$

We define the dissipation potential φ_p as

$$\varphi_p(\boldsymbol{\tau}) = \frac{\lambda_r^{1-p}}{p} \, |I_K^*(\boldsymbol{\tau})|^p, \; \boldsymbol{\tau} \in \mathcal{S}_3,$$

where λ_r and p are strictly positive material parameters; λ_r measures the material resistance and the exponent $p > 1$ is a viscosity measure. It is easy to prove that the polar function of φ_p is

$$\varphi_p^*(\boldsymbol{\tau}) = \frac{p-1}{p} \lambda_r |\theta(\boldsymbol{\tau})|^{\frac{p}{p-1}}. \tag{14}$$

Let us denote by $q = p/(p-1)$ the conjugate exponent of p; then expression (14) can be rewritten as

$$\varphi_p^*(\boldsymbol{\tau}) = \frac{1}{q} \lambda_r |\theta(\boldsymbol{\tau})|^q.$$

Replacing $\theta(\boldsymbol{\tau})$ defined by (13) in the previous expression, we obtain

$$\varphi_p^*(\boldsymbol{\tau}) = \frac{\theta_0}{q} |\boldsymbol{\tau}^D|^q, \tag{15}$$

where

$$\theta_0 = \frac{\lambda_r}{(\sqrt{2}k)^q}. \tag{16}$$

The classical Norton-Hoff law is formulated as

$$\dot{\boldsymbol{\varepsilon}}^{\mathrm{p}} \in \partial \varphi_p^*(\boldsymbol{\sigma}^D), \tag{17}$$

where $\partial \varphi_p^*(\boldsymbol{\sigma}^D)$ denotes the subdifferential of φ_p^* evaluated at $\boldsymbol{\sigma}^D$. Since φ_p^* is differentiable, its subdifferential coincides with its derivative, and therefore it results from (15)-(17) that

$$\dot{\boldsymbol{\varepsilon}}^{\mathrm{p}} = D\varphi_p^*(\boldsymbol{\sigma}^D) = \theta_0 \mid \boldsymbol{\sigma}^D \mid^{q-2} \boldsymbol{\sigma}^D. \tag{18}$$

If we superpose Hooke's law (9) for elastic strains and Norton-Hoff law (18) for viscoplastic ones, the resultant law, known as Maxwell-Norton law, is formulated as

$$\boldsymbol{\varepsilon}(\dot{\mathbf{u}}) = \overset{\cdot}{\overbrace{(\Lambda(T)\boldsymbol{\sigma})}} + D\varphi_p^*(\boldsymbol{\sigma}^D). \tag{19}$$

The Maxwell-Norton materials are an example of thermo-viscoelastic materials with long memory, as it was proved in Naya-Riveiro and Quintela [68].

– Creep under uniaxial loading. Let us consider the Maxwell-Norton law (19) in one dimension with constant parameters:

$$\dot{\varepsilon} = E\dot{\sigma} + \theta_o|\sigma|^{q-2}\sigma.$$

Let us justify that under a creep test, this law corresponds to the approximation shown in Figure 6. Indeed, if the solid is subjected to a constant stress $\sigma = \sigma_0 > 0$, then

$$\dot{\varepsilon} = \theta_o \sigma_0^{q-1},$$

and therefore,

$$\varepsilon(t) = \theta_o \sigma_0^{q-1} t + \varepsilon_0,$$

where ε_0 is the initial strain.

– Temperature dependence of strain rate. If we perform several creep tests at different temperatures, we can observe that the strain rate decreases when temperature increases (see Bower [27] or Lemaitre and Chaboche [61]). This temperature dependence of strain rate can be fit by the following coefficient of Arrhenius type:

$$e^{\frac{-G}{R(T+273)}},$$

where G is an activation energy and R is the Boltzmann constant. Therefore, to take into account this effect, we define

$$\kappa(T) = \theta_o e^{\frac{-G}{R(T+273)}}, \tag{20}$$

and we replace θ_0 by $\kappa(T)$ in expression (15). So, let us define the new viscoplastic function depending on temperature:

$$\Phi_q(\boldsymbol{\sigma}, T) = \frac{1}{q}\kappa(T)|\boldsymbol{\sigma}|^q, \ \boldsymbol{\sigma} \in \mathcal{S}_3, \ T \in \mathbb{R}.$$

Then, if we consider thermal law (10) and viscoplastic law (19), replacing φ_p^* by Φ_q, the resultant thermo-elastic-viscoplastic law (8) is rewritten as

$$\boldsymbol{\varepsilon}(\dot{\mathbf{u}}) = \overset{\cdot}{\overbrace{(\Lambda(T)\boldsymbol{\sigma})}} + D_\sigma\Phi_q(\boldsymbol{\sigma}^D, T) + \alpha(T)\dot{T}\mathbf{I},$$

where $D_\sigma\Phi_q$ denotes the derivative of Φ_q with respect to $\boldsymbol{\sigma}$ given by

$$D_\sigma\Phi_q(\boldsymbol{\sigma}^D, T) = \kappa(T)\left|\boldsymbol{\sigma}^D\right|^{q-2}\boldsymbol{\sigma}^D. \tag{21}$$

2.2.4 Problem (MP)

Summing up, the mechanical problem we must solve is the following:

Problem (MP):
Find the displacement field $\mathbf{u}(\mathbf{x},t)$ and the stress tensor field $\boldsymbol{\sigma}(\mathbf{x},t)$, at each point $\mathbf{x} \in \Omega_s(t)$ and at each instant $t \in (t_0, t_f]$ such that:

$$-\mathrm{Div}(\boldsymbol{\sigma}) = \mathbf{f} \quad \text{in} \quad \Omega_s(t), \tag{22}$$

$$\boldsymbol{\sigma}\mathbf{n} = p_r\mathbf{n} \quad \text{on} \quad \Gamma_{u,sl}(t), \tag{23}$$

$$\boldsymbol{\sigma}\mathbf{n} = \mathbf{0} \quad \text{on} \quad \Gamma_{u,n1}(t), \tag{24}$$

$$\boldsymbol{\sigma}_t = \mathbf{0},\ u_n = 0 \quad \text{on} \quad \Gamma_{u,n2}(t) \cup \Gamma_{u,s}(t), \tag{25}$$

$$\boldsymbol{\sigma}_t = \mathbf{0},\ \sigma_n \le 0,\ u_n \le 0,\ \sigma_n u_n = 0 \quad \text{on} \quad \Gamma_{u,c}, \tag{26}$$

$$\boldsymbol{\varepsilon}(\dot{\mathbf{u}}) = \overbrace{(A(T)\boldsymbol{\sigma})}^{\cdot} + D_\sigma \Phi_q(\boldsymbol{\sigma}^D, T) + \alpha(T)\dot{T}\,\mathbf{I} \quad \text{in} \quad \Omega_s(t), \tag{27}$$

$$\mathbf{u}(t_0) = \mathbf{u}_0,\ \ \boldsymbol{\sigma}(t_0) = \boldsymbol{\sigma}_0 \quad \text{in} \quad \Omega_s(t_0). \tag{28}$$

3 Mathematical analysis

This Section is devoted to the mathematical analysis of Problem (MP). Firstly, in Section 3.1 we present a summary of the relevant theoretical results for quasistatic thermo-mechanical problems for Maxwell-Norton materials. Secondly, in Section 3.2 we introduce a weak formulation and the necessary functional framework to do it. Section 3.3 is devoted to give an existence result for a simplified submodel of Problem (MP); it corresponds to an elastic-viscoplastic model for a Maxwell-Norton material with contact condition and posed over a time independent domain. Finally, in Section 3.4 we propose a new variational formulation adapted to the numerical simulation of the complete Problem (MP); the aim is to eliminate the metallostatic pressure on the interphase, modelling it as a gravity force on the liquid region.

3.1 State of art

In the literature there exist several existence results for viscoelastic problems of Maxwell-Norton type. Djaoua and Suquet [35] and Le Tallec [60] proved the existence of solution for Maxwell-Norton problems with classical mixed boundary conditions. Later, in Blanchard and Le Tallec [26], the proof given in [60] was extended to a Maxwell-Norton law with viscoelastic coefficients depending on time and space. Nevertheless, these results are not applicable to Problem (MP) since they use variational formulations in velocities, and their methodology does not work for formulations in displacements, which are necessary to include Signorini contact condition (26).

In [12] the authoresses proved a result of existence of solution for a submodel of Problem (MP), defined over a domain independent of time and

without considering the thermal effects. In that work, the proof was based in the result given in Djaoua and Suquet [35] for mixed boundary conditions, generalizing the existence result to include a Signorini contact condition. Later, in Barral *et al.* [6] this methodology was applied to prove the existence and uniqueness of solution when considering the thermal strain and coefficients depending on temperature in the behaviour law. In that result, it was assumed that $\dot{T} > 0$, so, it is not applicable for casting processes.

3.2 Variational inequality

In order to obtain a weak formulation of Problem (MP), we introduce a suitable framework to treat the nonlinearities due to the behaviour law and the contact condition. Following the functional framework for Norton-Hoff law studied by Geymonat and Suquet [46], we present the functional subsets of admissible displacements and stresses. Next, we introduce the hypotheses on the temperature field, the applied forces and the initial conditions, needed to define a variational formulation of Problem (MP) which involves an inequality due to the contact condition.

A detailed description of variational formulations for different contact problems can be found in Kikuchi and Oden [55] for elastic materials, Burguera and Viaño [28] for perfect plastic materials or in Glowinsky and Le Tallec [47] for some viscoplastic materials.

3.2.1 Functional framework

From now on, we assume that at each instant $t \in (t_0, t_f]$, $\Omega_s(t)$ is a smooth enough bounded domain in $\mathbb{R}^3$. Let us assume that the exponent of the viscoplastic law verifies $2 \leq q < +\infty$ and so its conjugate exponent p verifies $1 < p \leq 2$.

We consider the space of displacement fields as the following subspace of the standard Sobolev space $[W^{1,p}(\Omega_s(t))]^3$:

$$\mathbf{V}^p(t) = \{\mathbf{v} \in [W^{1,p}(\Omega_s(t))]^3;\ \mathrm{Div}(\mathbf{v}) \in L^2(\Omega_s(t))\},$$

which is a Banach space endowed with the norm

$$\|\mathbf{v}\|_{\mathbf{V}^p(t)} = \|\mathbf{v}\|_{[L^p(\Omega_s(t))]^3} + \|\boldsymbol{\varepsilon}^D(\mathbf{v})\|_{[L^p(\Omega_s(t))]^9} + \|\mathrm{Div}(\mathbf{v})\|_{L^2(\Omega_s(t))}.$$

Let $\mathbf{U}^p(t)$ be the subspace of $\mathbf{V}^p(t)$ obtained when considering the confinement by the mould of the mushy region and the symmetry condition (see equation (25)):

$$\mathbf{U}^p(t) = \{\mathbf{v} \in \mathbf{V}^p(t); v_n = 0 \text{ on } \Gamma_{u,n2}(t) \cup \Gamma_{u,s}(t)\}.$$

In order to take into account the contact condition (26), the subset of kinematically admissible displacements at each instant t is

$$\mathbf{U}^p_{ad}(t) = \{\mathbf{v} \in \mathbf{U}^p(t);\ v_n \leq 0 \text{ on } \Gamma_{u,c}\}.$$

We define the space of stress fields

$$\mathbf{X}^q(t) = \{\boldsymbol{\tau} = (\tau_{ij});\ \tau_{ij} = \tau_{ji},\ \boldsymbol{\tau}^D \in [L^q(\Omega_s(t))]^9,\ \mathrm{tr}(\boldsymbol{\tau}) \in L^2(\Omega_s(t))\},$$

which is a Banach space endowed with the norm

$$\|\boldsymbol{\tau}\|_{\mathbf{X}^q(t)} = \|\boldsymbol{\tau}^D\|_{[L^q(\Omega_s(t))]^9} + \|\mathrm{tr}(\boldsymbol{\tau})\|_{L^2(\Omega_s(t))}.$$

We introduce the subspace of $\mathbf{X}^q(t)$

$$\mathbf{H}^q(t) = \{\boldsymbol{\tau} \in \mathbf{X}^q(t);\ \mathrm{Div}(\boldsymbol{\tau}) \in [L^q(\Omega_s(t))]^3\},$$

which is also a Banach space endowed with the norm

$$\|\boldsymbol{\tau}\|_{\mathbf{H}^q(t)} = \|\boldsymbol{\tau}\|_{\mathbf{X}^q(t)} + \|\mathrm{Div}(\boldsymbol{\tau})\|_{[L^q(\Omega_s(t))]^3}.$$

In Geymonat and Suquet [46] it was proved that the space of distributions $[\mathcal{D}(\overline{\Omega}_s(t))]^9$ is dense in $\mathbf{H}^q(t)$. Moreover, the following Lemma was also proved:

Lemma 1 *The application*

$$\boldsymbol{\tau} \in \mathbf{H}^q(t) \to \boldsymbol{\tau}\mathbf{n} \in [W^{-\frac{1}{q},q}(\Gamma_u(t))]^3,$$

is linear and continuous. Moreover, the following Green's formula is verified:

$$\int_{\Omega_s(t)} \boldsymbol{\tau} : \boldsymbol{\varepsilon}(\mathbf{v})dx + \int_{\Omega_s(t)} \mathrm{Div}(\boldsymbol{\tau}) \cdot \mathbf{v}dx = \langle \boldsymbol{\tau}\mathbf{n}, \mathbf{v}\rangle_{\Gamma_u(t)}, \tag{29}$$

for all $\boldsymbol{\tau} \in \mathbf{H}^q(t)$ and $\mathbf{v} \in \mathbf{V}^p(t)$, where $\langle\cdot,\cdot\rangle_{\Gamma_u(t)}$ denotes the duality product between $[W^{-\frac{1}{q},q}(\Gamma_u(t))]^3$ and $[W^{1-\frac{1}{p},p}(\Gamma_u(t))]^3$.

3.2.2 Variational inequality. Problem (VMP)

From now on, we assume that the following hypotheses are satisfied:

- **(H1)** The viscoplastic exponent q verifies $2 \leq q < +\infty$, and its conjugate exponent p verifies $1 < p \leq 2$.
- **(H2)** The metallostatic pressure $p_r \in W^{1,\infty}(t_0, t_f; W^{-\frac{1}{q},q}(\Gamma_u(t)) \cap L^q(\Gamma_{u,sl}(t)))$; the volume forces $\mathbf{f} \in W^{1,\infty}(t_0, t_f; [L^q(\Omega_s(t))]^3)$ and the density is such that $\rho(s) \geq \rho_0 > 0$, $\forall s \in \mathbb{R}$.
- **(H3)** The elasticity tensor $\Lambda \in [W^{1,\infty}(\mathbb{R})]^{81}$ is symmetric and:

$$\exists\ \beta > 0;\ \Lambda\boldsymbol{\tau} : \boldsymbol{\tau} \geq \beta|\boldsymbol{\tau}|^2,\ \forall \boldsymbol{\tau} \in \mathcal{S}_3,\ \text{a.e. in } \mathbb{R}. \tag{30}$$

- **(H4)** $\boldsymbol{\sigma}_0 \in \mathbf{H}^q(t_0)$, $\mathbf{u}_0 \in \mathbf{V}^p(t_0)$ and verify the natural compatibility conditions.
- **(H5)** The temperature field $T \in W^{1,\infty}(t_0, t_f; L^\infty(\Omega_s(t)))$.
- **(H6)** The coefficient of thermal expansion $\alpha \in L^\infty(\mathbb{R})$ and the coefficient of the viscoplastic law $\kappa \in L^\infty(\mathbb{R})$.

Following the usual procedure, multiplying equation (22) by test functions in $\mathbf{U}^p_{ad}(t)$, integrating over $\Omega_s(t)$ and using Green's formula (29), the proposed variational formulation of Problem (MP) is:

Problem (VMP):
Find $\mathbf{u} \in W^{1,\infty}(t_0, t_f; \mathbf{U}^p_{ad}(t))$ and $\boldsymbol{\sigma} \in W^{1,\infty}(t_0, t_f; \mathbf{H}^q(t))$ such that *a.e.* $t \in (t_0, t_f]$

$$\int_{\Omega_s(t)} \boldsymbol{\sigma}(t) : \boldsymbol{\varepsilon}(\mathbf{v} - \mathbf{u}(t))\, dx \geq \int_{\Omega_s(t)} \mathbf{f}(t) \cdot (\mathbf{v} - \mathbf{u}(t))\, dx + \int_{\Gamma_{u,sl}(t)} p_r(t)\mathbf{n} \cdot (\mathbf{v} - \mathbf{u}(t))\, d\Gamma, \quad \forall \mathbf{v} \in \mathbf{U}^p_{ad}(t), \tag{31}$$

and verifying behaviour law (27) and initial conditions (28).

Remark 1 Notice that if the solution $\mathbf{u}(t)$, $\boldsymbol{\sigma}(t)$ is smooth enough, Problems (MP) and (VMP) are equivalent.

3.3 Existence of a solution for an elastic-viscoplastic problem of Maxwell-Norton type with contact condition

Due to the complexity of the mathematical analysis of the complete casting problem, throughout this subsection we restrict ourselves to the case where the mechanical domain is time independent and the behaviour law does not depend on temperature. Nevertheless, the numerical methodology presented in the remaining of the paper will deal with the complete casting problem.

In order to formulate the problem in a general frame, let us consider a continuous body which occupies at rest a bounded domain $\Omega_s \subset \mathbb{R}^3$, $\Omega_s \in \mathcal{C}^{1,1}$, corresponding to the solidified part of the aluminium slab. Its boundary $\Gamma_u = \partial\Omega_s$ is partitioned into three non-empty, disjoint and open parts $\Gamma_{u,d}$, $\Gamma_{u,n}$ and $\Gamma_{u,c}$ satisfying

$$\Gamma_u = \bar{\Gamma}_{u,d} \cup \bar{\Gamma}_{u,n} \cup \bar{\Gamma}_{u,c},$$

with $\text{meas}(\Gamma_{u,d}) > 0$. We consider the following boundary conditions:

- Due to the effect of the metallostatic pressure and the equilibrium of forces, it is reasonable to assume that the slab rests on the center of its base, $\Gamma_{u,d}$, that is,
$$\mathbf{u} = \mathbf{0} \text{ on } (t_0, t_f] \times \Gamma_{u,d}.$$
- $\Gamma_{u,c}$ denotes the remainder of the boundary between the slab and the bottom block, which is the region susceptible to be in contact; on this boundary, condition (26) is considered.

– $\Gamma_{u,n}$ denotes the lateral and upper faces; on this boundary, we consider traction surface forces of density $\mathbf{h}$:

$$\boldsymbol{\sigma}\mathbf{n} = \mathbf{h} \text{ on } (t_0, t_f] \times \Gamma_{u,n}.$$

Condition (23) due to the metallostatic pressure and Neumann condition (24) of Problem (MP) can be considered as a particular case of this Neumann condition.

Then, the problem we want to solve is:

Problem $(\widetilde{MP})$:
Find the displacement field $\mathbf{u}$ and the stress tensor $\boldsymbol{\sigma}$ verifying

$$-\mathrm{Div}(\boldsymbol{\sigma}) = \mathbf{f} \quad \text{in} \quad (t_0, t_f] \times \Omega_s, \tag{32}$$
$$\boldsymbol{\varepsilon}(\dot{\mathbf{u}}) = \Lambda\dot{\boldsymbol{\sigma}} + D_\sigma\Phi_q(\boldsymbol{\sigma}^D, T) \quad \text{in} \quad (t_0, t_f] \times \Omega_s, \tag{33}$$
$$\mathbf{u} = \mathbf{0} \quad \text{on} \quad (t_0, t_f] \times \Gamma_{u,d}, \tag{34}$$
$$\boldsymbol{\sigma}\mathbf{n} = \mathbf{h} \quad \text{on} \quad (t_0, t_f] \times \Gamma_{u,n}, \tag{35}$$
$$u_n \leq 0, \sigma_n \leq 0, \boldsymbol{\sigma}_t = \mathbf{0}, \sigma_n u_n = 0 \quad \text{on} \quad (t_0, t_f] \times \Gamma_{u,c}, \tag{36}$$
$$\mathbf{u}(t_0) = \mathbf{u}_0,\ \boldsymbol{\sigma}(t_0) = \boldsymbol{\sigma}_0 \quad \text{in} \quad \Omega_s. \tag{37}$$

In this section, we assume that the following hypotheses are satisfied:

$(\widetilde{\mathbf{H1}})$ The exponent q verifies $2 \leq q < 6$, and therefore $6/5 < p \leq 2$.
$(\widetilde{\mathbf{H2}})$ The applied forces satisfy

$$\mathbf{f} \in W^{2,\infty}(t_0, t_f; [L^q(\Omega_s)]^3),$$

$$\mathbf{h} \in W^{2,\infty}(t_0, t_f; [W^{-\frac{1}{q},q}(\Gamma_u)]^3 \cap [L^q(\Gamma_{u,n})]^3).$$

$(\widetilde{\mathbf{H3}})$ The elasticity tensor $\Lambda \in [L^\infty(\Omega_s)]^{81}$ is independent of time, symmetric and verifies (30).
$(\widetilde{\mathbf{H4}})$ $\boldsymbol{\sigma}_0 \in \mathbf{H}^q$, $\mathbf{u}_0 \in \mathbf{V}^p$ and verify the natural compatibility conditions, where $\mathbf{H}^q$ and $\mathbf{V}^p$ are defined in an analogous manner to $\mathbf{H}^q(t)$ and $\mathbf{V}^p(t)$ over the time independent domain Ω_s.

Hypothesis $(\widetilde{\mathbf{H1}})$ is satisfied by some aluminium alloys at high temperatures as shown in Wong and Jonas [85].

Theorem 1 *Under the above assumptions* $(\widetilde{\mathbf{H1}})$–$(\widetilde{\mathbf{H4}})$*, there exists a solution of Problem* $(\widetilde{MP})$*,* $(\mathbf{u}, \boldsymbol{\sigma}) \in W^{1,2}(t_0, t_f; \tilde{\mathbf{U}}^p_{ad}) \times \big(W^{1,2}(t_0, t_f; \mathbf{X}^2) \cap L^\infty(0, t_f; \mathbf{X}^q)\big)$*, where*

$$\tilde{\mathbf{U}}^p_{ad} = \{\mathbf{v} \in \mathbf{V}^p;\ \mathbf{v} = \mathbf{0} \text{ on } \Gamma_D\}.$$

Sketch of the proof: The proof of this theorem was given in [12]. There, the problem was discretized in time by using an implicit Euler scheme and a weak formulation in stresses was proposed. The existence of a unique stress solution of that weak problem was proved by means of the classic variational inequality theory (see Kinderlehrer and Stampacchia [57]); next, the corresponding discretized displacement field was reconstructed showing that the associated movement is free where there is a gap between the slab and the bottom block. Some estimates allowed to pass to the limit and finally, that limit was proved to be the solution of the continuous problem. This last step was the main difficulty in the proof since the contact condition did not allow to obtain the necessary orthogonality relations between strains and stresses which were essential in other papers such as Djaoua and Suquet [35] or Bensoussan and Frehse [17]. To overcome this difficulty, compensated compactness techniques were used thanks to the hemicontinuity and monotonicity of $D_\sigma \Phi_q$ (see Murat [67]). □

3.4 A variational formulation over the entire slab. A fictitious domain technique

Let us go back to the complete casting problem (MP). One of the main difficulties in its numerical solution is the right imposition of the metallostatic pressure exerted by the liquid metal on the recently solidified one. Remember that the upper boundary of the mechanical domain, $\Gamma_{u,sl}(t)$, is the isotherm corresponding to the liquidus temperature, which is the free boundary of the associated thermal problem. In order to impose numerically the metallostatic pressure on $\Gamma_{u,sl}(t)$, there exist at least three possibilities:

- modelling the behaviour of the entire slab, including the liquid metal;
- considering only the solid part and remeshing it at each time instant; or,
- extending this domain to the entire slab, but replacing the liquid metal by a very weak elastic material with the same density.

The first possibility requires the hydro-dynamical simulation of the liquid, which would complicate its numerical resolution. When applying the second possibility, called front tracking methods, the mechanical computational domain changes at each iteration, so remeshing is needed; furthermore, the discretization of its upper boundary, obtained from the thermal submodel, should be updated and consequently, the imposition of the metallostatic pressure would depend on how good the discretization of the outward normal is. In the third possibility, an extended problem is solved on a fixed domain, the entire slab; in particular, the liquid aluminium is replaced by a very weak elastic material under the action of the same gravity volume forces, so that it does not offer resistance to solid deformations and the weight of the liquid metal is correctly imposed (see [10,11] or Hannart *et al.* [50]). Another option, used in Agelet de Saracibar *et al.* [1] is to use a thermo-elastic-viscoplastic model, suitable for the solid-like phase, that degenerates into a pure thermo-viscous

model, suitable for the liquid-like phase, according to the evolution of a solid fraction function.

We have chosen the third possibility because it has the advantage that we only need to solve an elasticity problem in the liquid part and the metallostatic pressure would be correctly imposed on the boundary. Nevertheless, numerical simulations showed that it was not sufficient to consider a very weak elastic law in the fictitious domain, corresponding to the liquid region, since the solution was strongly dependent on the fictitious Lamé coefficients. In fact, for some choices of these coefficients the weight of the liquid metal was not locally recovered and shear stresses arose on the interface.

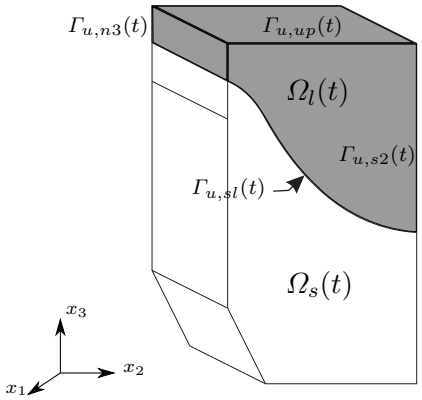

Fig. 7 Computational domain of the mechanical problem $\Omega_s(t)$ and fictitious domain $\Omega_l(t)$ (shading part).

In order to analyze the behaviour of the fictitious material in terms of its Lamé coefficients, in [10,11] an asymptotic analysis was carried out to obtain their optimal values.

Let $\Omega_l(t)$ denote the liquid zone of the slab at the instant t, that is,

$$\Omega_l(t) = \{\mathbf{x} \in \Omega(t); T(\mathbf{x}, t) > T_l\}.$$

At this region, we consider a very weak elastic material, whose Hooke's law depends on a small parameter ϵ,

$$\boldsymbol{\sigma}^\epsilon(\mathbf{u}^\epsilon) = \Lambda_l^{-1}\boldsymbol{\varepsilon}(\mathbf{u}^\epsilon) = \lambda_l^\epsilon \mathrm{Div}(\mathbf{u}^\epsilon)\mathbf{I} + 2\mu_l^\epsilon \boldsymbol{\varepsilon}(\mathbf{u}^\epsilon),$$

where its Lamé coefficients, $\lambda_l^\epsilon, \mu_l^\epsilon$, change with different length scale:

$$\lambda_l^\epsilon = \epsilon^\beta \overline{\lambda},\ \mu_l^\epsilon = \epsilon^\delta \overline{\mu}, \tag{38}$$

with $\overline{\lambda}$, $\overline{\mu}$, δ and β real positive numbers independent of ϵ. So, the fictitious material is assumed to be softer than the solid one.

We consider gravity volume forces with constant density $\rho_l = \rho(T_l)$ to impose rightly the weight of the liquid aluminium on the interface and so the metallostatic pressure there.

The boundary of $\Omega_l(t)$ is split into four disjoint open parts (see Figure 7):

$$\partial\Omega_l(t) = \bar{\Gamma}_{u,up}(t) \cup \bar{\Gamma}_{u,s2}(t) \cup \bar{\Gamma}_{u,n3}(t) \cup \bar{\Gamma}_{u,sl}(t),$$

where:

- $\Gamma_{u,up}(t)$ denotes the upper boundary which is free of forces;
- $\Gamma_{u,s2}(t)$ is the symmetry boundary; and
- $\Gamma_{u,n3}(t)$ corresponds to the outer lateral faces where the material is confined by the mould.

3.4.1 Asymptotic justification of the pressure treatment

In [10,11], an asymptotic expansion method was applied to compute the optimal Lamé coefficients, verifying relations (38), needed to impose correctly the metallostatic pressure. For every value of $\lambda_l^\epsilon, \mu_l^\epsilon$ the solution of Problem (VMP) was well approached far from the thermal free boundary $\Gamma_{u,sl}$; nevertheless, its behaviour near this boundary depended strongly on δ and β parameters:

- When $\delta > \beta$, this has the effect of applying locally the metallostatic pressure to the solidification front. Indeed, under suitable regularity assumptions on the data, in [11] the authoresses proved that, for linear elastic materials, the term of order zero of the asymptotic expansion with respect to ϵ, $\mathbf{u}^0$, when is restricted to $\Omega_s(t)$ verifies :

$$\boldsymbol{\sigma}(\mathbf{u}^0)\mathbf{n} = p_r\mathbf{n} \text{ on } \Gamma_{u,sl}.$$

- If $\delta \leq \beta$, shear stresses in the fictitious domain appear and, in general, the metallostatic pressure was not correctly imposed on $\Gamma_{u,sl}$. Nevertheless, if $\delta = \beta$ and $\overline{\lambda} >> \overline{\mu}$, shear stresses decrease and the approximation of the metallostatic pressure near $\Gamma_{u,sl}$ is better (see [10]).

These results are visualized in the following two-dimensional linear static test where we focus on the behaviour near the interface, eliminating the remaining difficulties of Problem (MP). Let Ω be a rectangle in the x_2x_3 plane, centered in $x_2 = 0$ and with width $w = 0.5\,\text{m}$ and height $h = 0.8\,\text{m}$. Let us assume that the temperature field is such that $\Gamma_{u,sl}$ is given by the expression:

$$\Gamma_{u,sl} = \{\mathbf{x} = (x_2, x_3); -4|x_2| + 5x_3 = 2\}.$$

The computational domain for this numerical example is shown in Figure 8. Following the boundary notation of Problem (MP), the boundary of Ω_s is split in four disjoint and open parts, $\partial\Omega_s = \bar{\Gamma}_{u,sl} \cup \bar{\Gamma}_{u,d} \cup \bar{\Gamma}_{u,n1} \cup \bar{\Gamma}_{u,n2}$, where:

- On the upper boundary $\Gamma_{u,sl}$ we consider the metallostatic pressure.

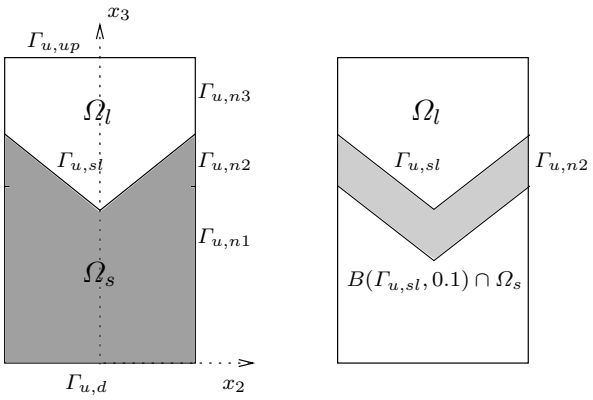

Fig. 8 Computational domain of Test ($T1$).

– On the base $\Gamma_{u,d}$, the following displacement is prescribed:

$$\mathbf{u} = \mathbf{u}_d(x_2) = \tilde{c}\,(-2hx_2, h^2 - x_2^2 - 0.85^2), \tag{39}$$

with

$$\tilde{c} = \frac{\rho g}{4(\lambda+\mu)},\ \rho = 2500\,\mathrm{kg/m^3},\ \lambda = 1.5e6\,\mathrm{N/m^2},\ \mu = 3.5e5\,\mathrm{N/m^2}.$$

– On $\Gamma_{u,n1} = \{\mathbf{x} \in \partial\Omega_s; 0 < x_3 < 0.5\}$ we impose a Neumann condition with surface force $\mathbf{h} = \rho g(x_3 - h)\mathbf{n}$.
– On $\Gamma_{u,n2} = \{\mathbf{x} \in \partial\Omega_s; 0.5 < x_3 < 0.6\}$ we assume that

$$\boldsymbol{\sigma}_t = \mathbf{0},\ u_n = \mathbf{u}_{sl} \cdot \mathbf{n}, \tag{40}$$

where

$$\mathbf{u}_{sl}(x_2, x_3) = \tilde{c}\,\left(2(x_3 - h)x_2, (x_3 - h)^2 - x_2^2 - 0.85^2\right). \tag{41}$$

This boundary condition substitutes confinement condition (25) in order to guarantee the continuity of the proposed solution.

So, the problem to solve is the following:

Test ($T1$):
Find $\mathbf{u}$ and $\boldsymbol{\sigma}$ such that

$$\begin{aligned} -\mathrm{Div}(\boldsymbol{\sigma}) &= \mathbf{f} \quad \text{in} \quad \Omega_s, \\ \boldsymbol{\sigma}\mathbf{n} &= p_r\mathbf{n} \quad \text{on} \quad \Gamma_{u,sl}, \\ \boldsymbol{\sigma}\mathbf{n} &= \mathbf{h} \quad \text{on} \quad \Gamma_{u,n1}, \\ \boldsymbol{\sigma}(\mathbf{u}) &= \lambda\,\mathrm{Div}(\mathbf{u})\mathbf{I} + 2\mu\,\boldsymbol{\varepsilon}(\mathbf{u}) \quad \text{in} \quad \Omega_s, \end{aligned}$$

and verifying boundary conditions (39) and (40) on $\Gamma_{u,d}$ and $\Gamma_{u,n2}$, respectively; with $\mathbf{f} = (0, 0, -\rho g)$ and $p_r = g(x_3 - h)$.

It is easy to prove that the solution of Test $(T1)$ is $\mathbf{u}_{sl}$, defined by expression (41), and $\boldsymbol{\sigma}(x_2, x_3) = \rho g(x_3 - h)\mathbf{I}$. This test is solved by using the MATLAB Partial Differential Equation Toolbox and the relative errors obtained are 2.8359e−4 in displacements and 5.1e−3 in stresses.

Next, we extend Test $(T1)$ to the entire domain Ω, applying the fictitious domain method explained in this section. Tables (1)-(3) show the relative errors in displacements and stresses for this numerical example, considering the following parameters:

$$\bar{\lambda} = 1e4\,\mathrm{N/m^2},\ \bar{\mu} = 10\,\mathrm{N/m^2}.$$

When $\delta < \beta$, the approximation is not good, even far from boundary Γ_{sl}, due to the occurrence of shear stresses in the fictitious domain (see Table 1 and Figure 9). When $\delta = \beta$ and $\overline{\lambda} >> \overline{\mu}$, the approximation of the solution restricted to Ω_s is quite good even near Γ_{sl}, since shear stresses are considerably reduced (see Table 2 and Figure 10). Finally, when $\delta > \beta$, the errors in displacements and stresses are of the same order than those obtained when solving directly Test $(T1)$ (see Table 3 and Figure 11); furthermore, in this case, the behaviour is similar regardless of the relationship between $\overline{\lambda}$ and $\overline{\mu}$.

Table 1 Relative errors when $\delta < \beta$ ($\delta = 1$, $\beta = 2$) for $\overline{\lambda} \gg \overline{\mu}$.

ϵ	Relative errors in Ω_s		Relative errors in $\Omega_s \setminus B(\Gamma_{u,sl}, 0.1)$	
	displacements	stresses	displacements	stresses
$1.0e-1$	0.0165	0.1184	0.0074	0.0181
$1.0e-3$	0.3499	1.9030	0.1556	0.4098
$1.0e-5$	0.4544	2.2573	0.1968	0.5252

Table 2 Relative errors when $\delta = \beta = 1$ for $\overline{\lambda} \gg \overline{\mu}$.

ϵ	Relative errors in Ω_s		Relative errors in $\Omega_s \setminus B(\Gamma_{u,sl}, 0.1)$	
	displacements	stresses	displacements	stresses
$1.0e-1$	$2.2e-3$	$2.56e-2$	$8.6770e-4$	$2.0e-3$
$1.0e-3$	$2.2e-3$	$2.56e-2$	$8.6824e-4$	$2.0e-3$
$1.0e-5$	$2.2e-3$	$2.56e-2$	$8.6824e-4$	$2.0e-3$

Table 3 Relative errors when $\delta > \beta$ ($\delta = 2$, $\beta = 1$) for $\overline{\lambda} \gg \overline{\mu}$.

ϵ	Relative errors in Ω_s		Relative errors in $\Omega_s \setminus B(\Gamma_{u,sl}, 0.1)$	
	displacements	stresses	displacements	stresses
$1.0e-1$	$4.6268e-4$	$4.9e-3$	$1.7727e-4$	$1.7e-3$
$1.0e-3$	$2.2322e-4$	$4.0e-3$	$1.7403e-4$	$1.6e-3$
$1.0e-5$	$2.2137e-4$	$4.0e-3$	$1.7404e-4$	$1.6e-3$

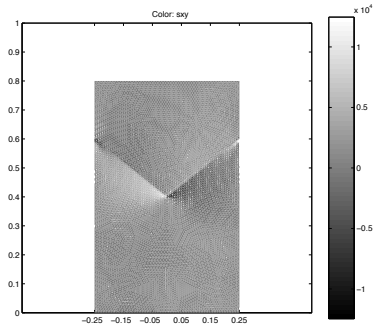

Fig. 9 Shear stresses for $\delta < \beta$ and $\overline{\lambda} >> \overline{\mu}$

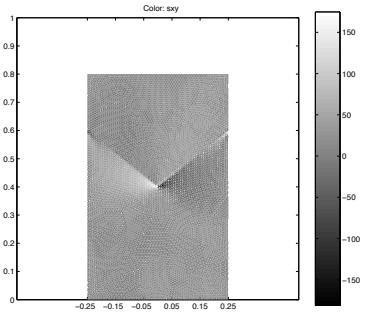

Fig. 10 Shear stresses for $\delta = \beta$ and $\overline{\lambda} >> \overline{\mu}$

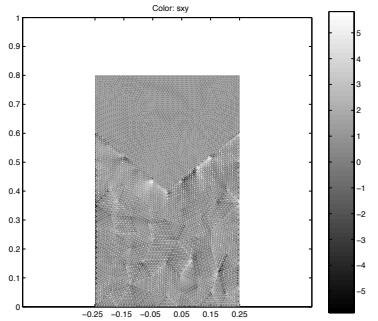

Fig. 11 Shear stresses for $\delta > \beta$ and $\overline{\lambda} >> \overline{\mu}$

3.4.2 Application of fictitious domain technique to Problem (VMP)

With the fictitious domain technique presented above, variational inequality (31) can be extended to the complete slab and the integral over the thermal free boundary $\Gamma_{u,sl}(t)$ disappears. Therefore, from now on, we will consider this new extended weak formulation over the entire slab $\Omega(t) = \text{int}(\bar{\Omega}_s(t) \cup \bar{\Omega}_l(t) \cup \bar{\Gamma}_{u,sl}(t))$. Furhermore, in order to simplify the notation, from now on, we omit the index ϵ in the behaviour law of the fictitious material.

Problem $(EVMP)$:
Find $\mathbf{u} \in W^{1,\infty}(t_0, t_f; \mathbf{U}^p_{ad}(t))$ and $\boldsymbol{\sigma} \in W^{1,\infty}(t_0, t_f; \mathbf{H}^q(t))$ verifying *a.e.* in $(t_0, t_f]$:

$$\int_{\Omega(t)} \boldsymbol{\sigma}(t) : \boldsymbol{\varepsilon}(\mathbf{v} - \mathbf{u}(t))\, dx \geq \int_{\Omega(t)} \mathbf{f}(t) \cdot (\mathbf{v} - \mathbf{u}(t))\, dx, \forall \mathbf{v} \in \mathbf{U}^p_{ad}(t), \tag{42}$$

$$\boldsymbol{\varepsilon}(\dot{\mathbf{u}})(t) = \begin{cases} \dot{\overbrace{(\Lambda(T)\boldsymbol{\sigma})}}(t) + \left(D_\sigma \Phi_q(\boldsymbol{\sigma}^D, T)\right)(t) + \left(\alpha(T)\dot{T}\right)(t)\mathbf{I} & \text{in } \Omega_s(t), \\ \dot{\overbrace{(\Lambda_l \boldsymbol{\sigma})}}(t) & \text{in } \Omega_l(t), \end{cases} \tag{43}$$

$$\mathbf{u}(t_0) = \mathbf{u}_0, \;\; \boldsymbol{\sigma}(t_0) = \boldsymbol{\sigma}_0, \text{ in } \Omega(t_0). \tag{44}$$

Remark 2 Notice that the functional spaces are extended to the entire slab in the natural way. The initial data, $\mathbf{u}_0$ and $\boldsymbol{\sigma}_0$, are also extended to all $\Omega(t_0)$, ensuring that the natural compatibility conditions are satisfied.

4 Numerical solution

This section is focused on the numerical solution of Problem $(EVMP)$. The three main difficulties to overcome are the following:

- The numerical solution of variational inequality (42) due to the contact condition. For that purpose, in [7] we proposed a Bermúdez-Moreno algorithm combined with a fixed point method. Afterwards, in [5] we improved this methodology by means of a generalized Newton method.
- The nonlinearity of behaviour law (43) in $\Omega_s(t)$. In order to avoid this nonlinearity, in [7] we also proposed the Bermúdez-Moreno algorithm and a fixed point method. Later, in [5] we considered a Newton method and finally, in [14] we presented a generalized Bermúdez-Moreno algorithm with variable parameters as the better option for the numerical approach of this law when it is combined with a contact condition like in casting processes simulation.
- The time dependence of the computational domain, which grows with time, and of its region with steep temperature gradients. To overcome this difficulty, meshes are adapted to the physics of the casting process.

In Section 4.1, a finite element discretization in space is introduced. Section 4.2 is devoted to the application of the standard Bermúdez-Moreno algorithm to solve, firstly, variational inequality (42) and, after, nonlinear behaviour law (43). There, an implicit Euler discretization in time is used. In Section 4.3 these algorithms are improved by using generalized Newton methods. Finally, in Section 4.4, a Bermúdez-Moreno algorithm with variable parameters for the numerical solution of the viscoplastic law is presented. Along all the section, several academic tests to analyze the efficiency of each of the presented algorithms are included. We show that choosing the Newton algorithm for contact and the Bermúdez-Moreno algorithm with variable parameters for viscoplasticity is the better option for the butt curl simulation of casting processes.

4.1 Discretization in space

A usual finite element approximation to discretize Problem $(EVMP)$ is considered. Displacements are discretized in space using the Lagrange finite element method of degree one and stresses are assumed constant within each element.

Let $\mathcal{T}_h(t)$ be a tetrahedral mesh of the computational domain, $\bar{\Omega}(t)$, compatible with the boundary partition. Throughout this section, h denotes the maximum diameter of $\mathcal{T}_h(t)$ and

$$\Sigma_h(t) = \{b_i\}_{1 \leq i \leq N_h(t)},$$

the nodes set of the tetrahedral mesh at time t. Moreover, $\mathcal{S}_h$ and $\mathcal{Z}_h(t)$ denote the triangulations induced on the contact boundary $\Gamma_{u,c}$ and on the boundaries $\Gamma_{u,n2}(t) \cup \Gamma_{u,n3}(t)$, respectively.

Let us define a family of finite dimensional subspaces of $\mathbf{V}^p(t)$ approximating the test functions $\mathbf{v}$ by piecewise polynomials of degree one over the mesh $\mathcal{T}_h(t)$:

$$\mathbf{V}_h(t) = \{\mathbf{v}_h \in [\mathcal{C}^0(\Omega(t))]^3; \mathbf{v}_h|_K \in [P_1(K)]^3, \forall K \in \mathcal{T}_h(t)\},$$
$$\mathbf{U}_h(t) = \{\mathbf{v}_h \in \mathbf{V}_h(t); (v_h)_\alpha = 0 \text{ on } [x_\alpha = 0],\ \mathbf{v}_h|_C \cdot \mathbf{n}|_C = 0, \forall C \in \mathcal{Z}_h(t)\},$$

where $P_i(K)$ denotes the space of polynomials of degree i defined on K and $\mathbf{v}_h|_C$ (resp. $\mathbf{n}|_C$) denotes the value of $\mathbf{v}_h$ (resp. $\mathbf{n}$) at the barycenter of C. Therefore, the discrete space of admissible displacements is

$$\mathbf{U}_{ad_h}(t) = \{\mathbf{v}_h \in \mathbf{U}_h(t); \mathbf{v}_h|_C \cdot \mathbf{n}|_C \leq 0, \forall C \in \mathcal{S}_h\}.$$

We denote by $\mathbf{X}_h(t)$ the discretized space of stresses

$$\mathbf{X}_h(t) = \{\boldsymbol{\xi}_h; (\xi_h)_{ij} = (\xi_h)_{ji}, \boldsymbol{\xi}_h|_K \in [P_0(K)]^9, \forall K \in \mathcal{T}_h(t)\}.$$

In $\mathbf{X}_h(t)$, we consider the norm induced by $\left[L^2(\Omega(t))\right]^9$.

Functions $\mathbf{v}_h \in \mathbf{V}_h(t)$ are characterized for their values in the vertices of the elements,

$$\mathbf{v}_h(x) = \sum_{i=1}^{N_h(t)} \mathbf{v}_h(b_i)\phi_i(x),$$

where $\{\phi_i\}_{i=1,\ldots,N_h(t)}$ are the usual shape functions verifying

$$\phi_i(b_j) = \delta_{ij},\ 1 \leq j \leq N_h(t).$$

Elements $\boldsymbol{\xi}_h \in \mathbf{X}_h(t)$ are characterized for their value at the barycenter of each element,

$$\boldsymbol{\xi}_h(x) = \sum_{K \in \mathcal{T}_h(t)} \boldsymbol{\xi}_h|_K \mathcal{X}_K(x),$$

$\mathcal{X}_K$ being the characteristic function of the element K. Moreover, at each time instant we consider the operator

$$\begin{aligned} \boldsymbol{\varepsilon}_h : \mathbf{V}_h(t) &\longrightarrow \mathbf{X}_h(t) \\ \mathbf{v}_h &\longrightarrow \boldsymbol{\varepsilon}_h(\mathbf{v}_h) = \sum_{K \in \mathcal{T}_h(t)} \boldsymbol{\varepsilon}(\mathbf{v}_h|_K)\mathcal{X}_K. \end{aligned}$$

Finally, T_h denotes the discretized temperature field obtained from the numerical simulation of the thermal problem; although for that problem the temperature field is computed using an analogous space discretization to that of $\mathbf{V}_h(t)$, in the mechanical simulation it is considered constant by element (see Bermúdez and Otero [23]).

With this notation, the discretized variational formulation corresponding to Problem $(EVMP)$ is the following:

Problem $(DEMP)$:
Find $\mathbf{u}_h \in W^{1,\infty}(t_0,t_f;\mathbf{U}_{ad_h}(t))$ and $\boldsymbol{\sigma}_h \in W^{1,\infty}(t_0,t_f;\mathbf{X}_h(t))$ verifying in $(t_0,t_f]$:

$$\int_{\Omega(t)} \boldsymbol{\sigma}_h(t) : \boldsymbol{\varepsilon}_h(\mathbf{v}_h - \mathbf{u}_h(t))\,dx \geq \int_{\Omega(t)} \mathbf{f}_h(t)\cdot(\mathbf{v}_h - \mathbf{u}_h(t))\,dx, \forall \mathbf{v}_h \in \mathbf{U}_{ad_h}(t), \tag{45}$$

$$\boldsymbol{\varepsilon}_h(\dot{\mathbf{u}}_h)(t) = \begin{cases} \overset{\cdot}{\overbrace{(\Lambda(T_h)\boldsymbol{\sigma}_h)}}(t) + \left(D_\sigma \Phi_q(\boldsymbol{\sigma}_h^D, T_h)\right)(t) \\ \quad + \left(\alpha(T_h)\dot{T}_h\right)(t)\mathbf{I} & \text{in } \Omega_{sh}(t), \\ \overset{\cdot}{\overbrace{(\Lambda_l\boldsymbol{\sigma}_h)}}(t) & \text{in } \Omega_{lh}(t), \end{cases} \tag{46}$$

$$\mathbf{u}_h(t_0) = \mathbf{u}_{0h}, \;\; \boldsymbol{\sigma}_h(t_0) = \boldsymbol{\sigma}_{0h} \text{ in } \Omega(t_0), \tag{47}$$

where $\Omega_{sh}(t) = \Omega_s(t) \cap \mathcal{T}_h(t)$ and $\Omega_{lh}(t) = \Omega_l(t) \cap \mathcal{T}_h(t)$.

4.2 Standard Bermúdez-Moreno algorithm

An overview of different numerical methods to solve contact problems can be found in Kikuchi and Oden [55], Wriggers [86] or in LeTallec [60] and references therein for viscoplastic laws. A simple way to deal with these nonlinearities is to use the well-known Bermúdez-Moreno lemma (see Bermúdez and Moreno [19]). This lemma has been widely applied not only in the numerical solution of this type of nonlinearities in solid mechanics (see Burguera and Viaño [28]) but also in such diverse scientific areas as finances (see Bermúdez *et al.* [22]), sediment transport (see Morales de Luna *et al.* [63]) or electromagnestism (see Bermúdez *et al* [18]). The application of Bermúdez-Moreno lemma to Problem $(DEMP)$ is the main idea of the algorithm developed by the authoresses in [7] which is summarized in the following.

4.2.1 Dealing with contact nonlinearity

In order to deal with variational inequality (45), we introduce the following notations:

$$E_h = \{p_h \in L^\infty(\Gamma_{u,c});\; p_h|_C \in P_0(C),\; \forall C \in \mathcal{S}_h\},$$
$$Q_h = \{p_h \in E_h;\; p_h|_C \leq 0,\; \forall C \in \mathcal{S}_h\}.$$

Let $G = \partial I_{Q_h}$ be the subdifferential of the indicator function of the closed convex Q_h defined in the Hilbert space E_h, which is a maximal monotone operator. We denote by $G^{\gamma_c} = G - \gamma_c \mathbf{I}$ its perturbed operator, with γ_c a real

positive parameter. To take into account the nonlinearity due to the contact condition, we define a Lagrange multiplier, called contact multiplier, as

$$p_h = G^{\gamma_c}\left((u_h)_n\right). \tag{48}$$

Applying Bermúdez-Moreno lemma, expression (48) is equivalent to

$$p_h = G^{\gamma_c}_{\lambda_c}\left((u_h)_n + \lambda_c\, p_h\right), \tag{49}$$

where $G^{\gamma_c}_{\lambda_c}$ is the Yosida approximation of G^{γ_c}, with λ_c, γ_c verifying that $\lambda_c > 0$, $0 \leq \lambda_c\gamma_c < 1$.
In [7], the following expression for $G^{\gamma_c}_{\lambda_c}$ was obtained:

$$G^{\gamma_c}_{\lambda_c}(\varphi_h) = \frac{1}{\lambda_c}\left(\varphi_h - \Pi_{Q_h}\left(\frac{1}{1-\lambda_c\gamma_c}\varphi_h\right)\right),\ \varphi_h \in E_h, \tag{50}$$

where Π_{Q_h} is the orthogonal projection over Q_h given by

$$\Pi_{Q_h}(p_h) = \begin{cases} p_h & \text{if } p_h \leq 0, \\ 0 & \text{if } p_h > 0, \end{cases}$$

p_h belonging to E_h. Furthermore, it was also proved that every solution of Problem $(DEMP)$ is a solution of the following problem which is formulated as a weak equality:

Problem $(DEMP_C)$:
Find $\mathbf{u}_h \in W^{1,\infty}(t_0, t_f; \mathbf{U}_{ad_h}(t))$, $\boldsymbol{\sigma}_h \in W^{1,\infty}(t_0, t_f; \mathbf{X}_h(t))$ and $p_h \in W^{1,\infty}(t_0, t_f; E_h)$ verifying in $(t_0, t_f]$

$$\int_{\Omega(t)} \boldsymbol{\sigma}_h(t) : \boldsymbol{\varepsilon}_h(\mathbf{v}_h)dx + \int_{\Gamma_{u,c}} \gamma_c(u_h)_n(v_h)_n d\Gamma = \int_{\Omega(t)} \mathbf{f}_h(t)\cdot\mathbf{v}_h dx - \int_{\Gamma_{u,c}} p_h(t)\,(v_h)_n d\Gamma,\ \forall \mathbf{v}_h \in \mathbf{U}_h(t), \tag{51}$$

$$p_h(t) = G^{\gamma_c}_{\lambda_c}((u_h)_n + \lambda_c\, p_h(t)) \text{ on } S_h, \tag{52}$$

together with behaviour law (46) and initial conditions (47).

To simplify the notation, from now on we will omit the index h to denote the elements of the discretized spaces.

4.2.2 Dealing with the nonlinear behaviour law

In order to introduce an iterative algorithm to deal with the nonlinear behaviour law, firstly we discretize it in time and then we apply again the Bermúdez-Moreno algorithm. For time discretization, we consider the following regular partition of the time interval:

$$t^0 = t_0,\ t^{j+1} = t^j + \Delta t,\ j = 0, ..., N-1,\ \Delta t = \frac{t_f - t_0}{N}.$$

From now on we denote by g^j an approximation of a given function $g(t)$ at time t^j.

By using an implicit Euler scheme, the time discretization of behaviour law (46) is

$$\boldsymbol{\varepsilon}(\mathbf{u}^{j+1}) - \boldsymbol{\varepsilon}(\mathbf{u}^j) = \begin{cases} \left(\Lambda(T^{j+1})\boldsymbol{\sigma}^{j+1} - \Lambda(T^j)\boldsymbol{\sigma}^j\right) + \alpha(T^{j+1})(T^{j+1} - T^j)\mathbf{I} \\ \quad +\Delta t\ D_\sigma \Phi_q \left(\left(\boldsymbol{\sigma}^{j+1}\right)^D, T^{j+1}\right) \text{ in } \Omega_s^{j+1}, \\ \\ \Lambda_l \boldsymbol{\sigma}^{j+1} - \Lambda_l \boldsymbol{\sigma}^j \text{ in } \Omega_l^{j+1}. \end{cases}$$

Next, in the following lemma, our objective is to obtain an explicit expression for $\boldsymbol{\sigma}^{j+1}$ in order to be replaced in mixed variational formulation (51). To do that, we define the viscoplastic multiplier $\mathbf{q}^{j+1}$ at the time step t^{j+1} as the perturbed operator of $D_\sigma \Phi_q$ at $\left(\boldsymbol{\sigma}^{j+1}\right)^D$ with parameter $\gamma_p \geq 0$:

$$\mathbf{q}^{j+1} = (D_\sigma \Phi_q)^{\gamma_p} \left(\left(\boldsymbol{\sigma}^{j+1}\right)^D, T^{j+1}\right). \tag{53}$$

Lemma 2 *At each time step t^{j+1}, $j = 0, \ldots, N-1$, known T^{j+1}, the stress tensor in Ω_s^{j+1} is given by the relation*

$$\boldsymbol{\sigma}^{j+1} = \mathcal{V}(T^{j+1}) \left(\boldsymbol{\varepsilon}(\mathbf{u}^{j+1}) - \Delta t \mathbf{q}^{j+1} + \frac{\Delta t \gamma_p s^{j+1}}{3} \mathrm{tr}(\boldsymbol{\varepsilon}(\mathbf{u}^{j+1}))\mathbf{I} + \mathbf{F}^j\right), \tag{54}$$

where $\mathbf{q}^{j+1}$ is defined by expression (53) and

$$\mathbf{F}^j = -\boldsymbol{\varepsilon}(\mathbf{u}^j) + \Lambda(T^j)\boldsymbol{\sigma}^j - \alpha(T^{j+1})(T^{j+1} - T^j)\left(1 + \Delta t \gamma_p s^{j+1}\right)\mathbf{I} + \frac{\Delta t \gamma_p s^{j+1}}{3}\left(\frac{1}{s^j}\mathrm{tr}(\boldsymbol{\sigma}^j) - \mathrm{tr}(\boldsymbol{\varepsilon}(\mathbf{u}^j))\right)\mathbf{I}, \tag{55}$$

with

$$s^j = \frac{E(T^j)}{1 - 2\nu(T^j)}.$$

In (54), the automorphism $\mathcal{V}(T)$ is defined by

$$\mathcal{V}(T)\boldsymbol{\tau} = \widetilde{\lambda}(T)\mathrm{tr}(\boldsymbol{\tau})\mathbf{I} + 2\widetilde{\mu}(T)\boldsymbol{\tau},$$

being

$$\widetilde{\lambda}(T) = \frac{E(T)\nu(T)}{(L(T) - 2\nu(T))(L(T) + \nu(T))},\ \ \widetilde{\mu}(T) = \frac{E(T)}{2(L(T) + \nu(T))},$$

and $L(T) = 1 + \gamma_p E(T)\Delta t$.

The proof of this lemma can be found in [3]. Notice that $\mathbf{F}^j$ represents the history of the solidified alloy up to time t^j and it also includes the expansional effects of the temperature changes at the time interval $[t^j, t^{j+1}]$.

In the following lemma the Bermúdez-Moreno method is applied to compute the viscoplastic multiplier.

Lemma 3 *At each time step t^{j+1} and given T^{j+1}, $j = 0, \ldots, N-1$, the viscoplastic multiplier $\mathbf{q}^{j+1}$ is a fixed point of the equation*

$$\mathbf{q}^{j+1} = (D_\sigma \Phi_q)_{\lambda_p}^{\gamma_p} \left(\left(\boldsymbol{\sigma}^{j+1}\right)^D + \lambda_p \mathbf{q}^{j+1}, T^{j+1} \right), \tag{56}$$

for λ_p a real positive number such that $0 \leq \lambda_p \gamma_p < 1$. In this equation, $(D_\sigma \Phi_q)_{\lambda_p}^{\gamma_p}$ denotes the Yosida approximation of $(D_\sigma \Phi_q)^{\gamma_p}$, which is given by

$$(D_\sigma \Phi_q)_{\lambda_p}^{\gamma_p}(\boldsymbol{\zeta}, T) = \frac{\boldsymbol{\zeta}}{\lambda_p} \left(1 - \frac{1}{\eta(1-\lambda_p\gamma_p)} \right), \ \boldsymbol{\zeta} \in \mathcal{S}_3, \ T \in \mathbb{R},$$

where $\eta = \eta(\boldsymbol{\zeta}, T)$ is the unique root of the equation

$$\eta^{q-1} - \eta^{q-2} - \frac{\lambda_p \kappa(T)}{(1-\lambda_p\gamma_p)^{q-1}} |\boldsymbol{\zeta}|^{q-2} = 0,$$

in the interval $[1, +\infty)$.

4.2.3 SBM algorithm

Here we summarize the standard Bermúdez-Moreno algorithm combined with a fixed method for the numerical simulation of Problem $(DEMP)$.

SBM1 Let $(\mathbf{u}^0, \boldsymbol{\sigma}^0)$ be given. We consider p^0 as the weight of the metal column over each face on the contact boundary and $\mathbf{q}^0 = \kappa(T^0) \left|(\boldsymbol{\sigma}^0)^D\right|^{q-2} (\boldsymbol{\sigma}^0)^D$.

SBM2 Then, for $j \geq 0$, $(\mathbf{u}^j,\ \boldsymbol{\sigma}^j,\ \mathbf{q}^j,\ p^j)$ known at time t^j, we determine $(\mathbf{u}^{j+1}, \boldsymbol{\sigma}^{j+1},\ \mathbf{q}^{j+1},\ p^{j+1})$ at time t^{j+1} by using the following iterative algorithm:

(a) Initialize $\mathbf{u}_0^{j+1} = \mathbf{u}^j$, $p_0^{j+1} = p^j$ and

$$\mathbf{q}_0^{j+1} = \begin{cases} \mathbf{q}^j & \text{in } \Omega_s^j, \\ \mathbf{0} & \text{in } \Omega^{j+1} \backslash \Omega_s^j. \end{cases}$$

(b) With $\mathbf{q}_{k-1}^{j+1}$, p_{k-1}^{j+1} known, compute $\mathbf{u}_k^{j+1}$ with $k \geq 1$ by solving the variational equality

$$\begin{aligned} &\int_{\Omega_s^{j+1}} \mathcal{V}(T^{j+1}) \left[\boldsymbol{\varepsilon}(\mathbf{u}_k^{j+1}) + \frac{\Delta t \gamma_p s^{j+1}}{3} \mathrm{tr}(\boldsymbol{\varepsilon}(\mathbf{u}_k^{j+1}))\mathbf{I} \right] : \boldsymbol{\varepsilon}(\mathbf{v}) dx + \\ &\int_{\Omega_l^{j+1}} \Lambda_l^{-1} \boldsymbol{\varepsilon}(\mathbf{u}_k^{j+1}) : \boldsymbol{\varepsilon}(\mathbf{v}) dx + \int_{\Gamma_{u,c}} \gamma_c \left(u_k^{j+1} \right)_n v_n d\Gamma = \\ &\int_{\Omega_s^{j+1}} \left[\mathcal{V}(T^{j+1}) \left(\Delta t \mathbf{q}_{k-1}^{j+1} - \mathbf{F}^j \right) \right] : \boldsymbol{\varepsilon}(\mathbf{v}) dx - \int_{\Gamma_{u,c}} p_{k-1}^{j+1} \, v_n d\Gamma + \\ &\int_{\Omega^{j+1}} \mathbf{f}^{j+1} \cdot \mathbf{v} dx, \quad \forall \mathbf{v} \in \mathbf{U}_h(t^{j+1}), \end{aligned} \tag{57}$$

where $\mathbf{F}^j$ is given by expression (55).

(c) The updated stress tensor is defined by

$$\boldsymbol{\sigma}_k^{j+1} = \begin{cases} \mathcal{V}(T^{j+1}) \left(\boldsymbol{\varepsilon}(\mathbf{u}_k^{j+1}) - \Delta t \mathbf{q}_{k-1}^{j+1} \right) \\ \quad + \mathcal{V}(T^{j+1}) \left(\dfrac{\Delta t \gamma_p s^{j+1}}{3} \mathrm{tr}(\boldsymbol{\varepsilon}(\mathbf{u}_k^{j+1})) \mathbf{I} + \mathbf{F}^j \right) & \text{in } \Omega_s^{j+1}, \\ \\ \Lambda_l^{-1} \boldsymbol{\varepsilon}(\mathbf{u}_k^{j+1}) & \text{in } \Omega_l^{j+1}. \end{cases}$$

(d) The updated contact multiplier is computed as

$$p_k^{j+1} = \frac{1}{\lambda_c} \left[\left(u_k^{j+1} \right)_n + \lambda_c p_{k-1}^{j+1} - \Pi_{Q_h} \left(\frac{\left(u_k^{j+1} \right)_n + \lambda_c p_{k-1}^{j+1}}{1 - \lambda_c \gamma_c} \right) \right].$$

(e) The updated viscoplastic multiplier is given by

$$\mathbf{q}_k^{j+1} = \frac{\left(\boldsymbol{\sigma}_k^{j+1} \right)^D + \lambda_p \mathbf{q}_{k-1}^{j+1}}{\lambda_p} \left(1 - \frac{1}{\eta_k^{j+1} (1 - \lambda_p \gamma_p)} \right),$$

in Ω_s^{j+1}, where

$$\eta_k^{j+1} = \eta \left(\left(\boldsymbol{\sigma}_k^{j+1} \right)^D + \lambda_p \mathbf{q}_{k-1}^{j+1}, T^{j+1} \right),$$

is the solution in the interval $[1, +\infty)$ of equation

$$\eta^{q-1} - \eta^{q-2} - \frac{\lambda_p \kappa(T^{j+1})}{(1 - \lambda_p \gamma_p)^{q-1}} \left| \left(\boldsymbol{\sigma}_k^{j+1} \right)^D + \lambda_p \mathbf{q}_{k-1}^{j+1} \right|^{q-2} = 0.$$

Remark 3 The only difficulty remaining in variational formulation (57) is how to impose the confinement condition on the liquid and mushy zones in three-dimensional simulations, since the transversal section of the slab is not rectangular, which implies a coupling between the components of the displacement field. This difficulty is overcome by using a penalization technique on these boundaries.

Remark 4 In practice, updating the contact and viscoplastic multipliers is performed with a relaxation parameter ϑ. For example, the updated viscoplastic multiplier is obtained after SBM2(e) by formula

$$\mathbf{q}_k^{j+1} = \vartheta \mathbf{q}_k^{j+1} + (1 - \vartheta) \mathbf{q}_{k-1}^{j+1}, \quad 0 < \vartheta \leq 1.$$

4.3 Newton algorithm

The SBM algorithm presented in Section 4.2 is robust and converges well in academic tests. Nevertheless, the greater the problem's magnitude, the slower its convergence. In casting processes, in which we must join two nonlinearities -contact and viscoplasticity-, this difficulty becomes more apparent. Furthermore, when it was applied to the simulation of the butt-curl deformation, its convergence got worse due to its strong dependence on the parameters and the large thermal stresses. In order to improve its convergence and to reduce the cpu-time, it was necessary to find efficient strategies. Concretely, in this section Newton methods to compute both contact and viscoplastic multipliers are introduced.

4.3.1 Dealing with contact nonlinearity

In this subsection we propose to use a generalized Newton method, based on the Lipschitzian properties of maximal monotone operators to improve the computation of the contact multiplier (see Facchinei and Pang [41], Pang [72] and Robinson [75]). The results in this section have been proved in [5].

Let us consider again Problem $(DEMP_C)$ with $\gamma_c = 0$ and $\lambda_c > 0$. In this case, the contact multiplier is obtained from the Yosida approximation of G (see equation (50)):

$$G_{\lambda_c}(\varphi) = \frac{1}{\lambda_c}\left(I - \Pi_{Q_h}\right)(\varphi),\ \varphi \in E_h. \tag{58}$$

Notice that at each $\varphi \in E_h$,

$$G_{\lambda_c}(\varphi)_{|C} = \hat{G}_{\lambda_c}(\varphi_{|C}),\ \forall C \in \mathcal{S}_h,$$

where

$$\hat{G}_{\lambda_c}(s) = \begin{cases} 0, & \text{if } s \le 0, \\ s/\lambda_c, & \text{if } s > 0, \end{cases} \tag{59}$$

at each point $s \in \mathbb{R}$. Moreover, $\hat{G}_{\lambda_c}$ is differentiable at each point $s \neq 0$.

Lemma 4 *At each point $s_0 \in \mathbb{R}$, the following approximation for $\hat{G}_{\lambda_c}(s_0)$ holds true:*

$$\hat{G}_{\lambda_c}(s_0) \cong \hat{G}_{\lambda_c}(s_1) + \begin{cases} 0, & \text{if } s_0 < 0, \\ -V s_1, & \text{if } s_0 = 0, \\ (s_0 - s_1)/\lambda_c, & \text{if } s_0 > 0, \end{cases} \tag{60}$$

for $s_1 \in \mathbb{R}$ close enough to s_0, and V belonging to the subdifferential $\partial \hat{G}_{\lambda_c}(s_0)$. Furthermore, the error of this approximation is of order $O\left(|s_0 - s_1|^2\right)$.

It is easy to prove that

$$\partial \hat{G}_{\lambda_c}(0) = \left[0, \frac{1}{\lambda_c}\right].$$

To solve numerically the contact problem we choose the null value for this subdifferential and so $V = 0$ in (60).

Then, the algorithm proposed to approach equations (51) and (52) at time t^{j+1} and iteration k is

$$\int_{\Omega^{j+1}} \boldsymbol{\sigma}_k^{j+1} : \boldsymbol{\varepsilon}(\mathbf{v}) dx + \int_{\Gamma_{u,c}} p_k^{j+1}\ v_n d\gamma = \int_{\Omega^{j+1}} \mathbf{f}^{j+1} \cdot \mathbf{v} dx,\ \forall \mathbf{v} \in \mathbf{U}_h(t^{j+1}), \tag{61}$$

$$p_k^{j+1} = p_{k-\frac{1}{2}}^{j+1} + \begin{cases} 0, & \text{if } s_{k-1}^{j+1} \leq 0, \\ \left(s_k^{j+1} - s_{k-1}^{j+1}\right)/\lambda_c, & \text{if } s_{k-1}^{j+1} > 0, \end{cases} \tag{62}$$

where

$$\begin{aligned} p_{k-\frac{1}{2}}^{j+1} &= \hat{G}_{\lambda_c}(s_{k-1}^{j+1}), \\ s_k^{j+1} &= \left(u_k^{j+1}\right)_n + \lambda_c\, p_k^{j+1}, \end{aligned} \tag{63}$$

choosing $s_1 = s_{k-1}^{j+1}$, $s_0 = s_k^{j+1}$ and $V = 0$ for $s_0 = 0$ in (60).

Remark 5 Note that at each iteration the variational equality corresponding to (61) is equivalent to the linear problem

$$\begin{aligned} -\text{Div}\left(\boldsymbol{\sigma}_k^{j+1}\right) &= \mathbf{f}^{j+1} \text{ in } \Omega^{j+1}, \\ \boldsymbol{\sigma}_k^{j+1}\mathbf{n} &= \mathbf{0} \text{ on } \Gamma_{u,n1}^{j+1} \cup \Gamma_{u,up}^{j+1}, \\ (\sigma_k^{j+1})_n = -p_k^{j+1},\ (\boldsymbol{\sigma}_k^{j+1})_t &= \mathbf{0} \text{ on } \Gamma_{u,c}, \\ (u_k^{j+1})_n = 0,\ (\boldsymbol{\sigma}_k^{j+1})_t &= \mathbf{0} \text{ on the remaining.} \end{aligned} \tag{64}$$

So, the contact multiplier p_k^{j+1} represents the obstacle reaction on $\Gamma_{u,c}$.

When analyzing formulae (61)-(63), we notice that there exists a coupling between the displacements and the contact multiplier on the boundary $\Gamma_{u,c}$. In order to overcome this difficulty, in [5] the following lemma was proved.

Lemma 5 *Let us consider the following sets:*

$$(\Gamma_{u,c,k}^{-})^{j+1} = \{C \in S_h;\ s_k^{j+1} \leq 0\}, \tag{65}$$

$$(\Gamma_{u,c,k}^{+})^{j+1} = \{C \in S_h;\ s_k^{j+1} > 0\}. \tag{66}$$

Then,

$$\begin{aligned} p_k^{j+1} &= 0 \ \textit{on}\ (\Gamma_{u,c,k-1}^{-})^{j+1}, \\ \left(u_k^{j+1}\right)_n &= 0 \ \textit{on}\ (\Gamma_{u,c,k-1}^{+})^{j+1}. \end{aligned} \tag{67}$$

Thus, at each iteration, the boundary $\Gamma_{u,c}$ is split into two parts:

- $(\Gamma^{+}_{u,c,k-1})^{j+1}$, where the normal displacements and the tangential component of stresses are null and the normal stress depends only on the contact multiplier; and
- $(\Gamma^{-}_{u,c,k-1})^{j+1}$, where the normal and tangential stresses are null.

Notice that this division of $\Gamma_{u,c}$ is the only variable modified at each iteration.

There are several ways to achieve the solution using formulae (61)-(63), but since our objective is to couple the contact effects with the viscoplastic ones, we propose an algorithm based on two steps thanks to equations (64) and (67) (see [5] for details). In particular, condition (67) at each iteration is imposed by a penalty term with small parameter, ϵ_c, on the faces with effective contact $(\Gamma^{+}_{u,c,k-1})^{j+1}$, with $\lambda_c \geq 1$:

$$\int_{\Omega^{j+1}} \boldsymbol{\sigma}_k^{j+1} : \boldsymbol{\varepsilon}(\mathbf{v})\, dx + \frac{1}{\epsilon_c} \int_{\left(\Gamma^{+}_{u,c,k-1}\right)^{j+1}} (u_k^{j+1})_n v_n = \int_{\Omega^{j+1}} \mathbf{f}^{j+1} \cdot \mathbf{v}\, dx, \quad (68)$$

for all $\mathbf{v} \in \mathbf{U}_h(t^{j+1})$, and the contact multiplier is updated by

$$p_k^{j+1} = \begin{cases} \dfrac{1}{\epsilon_c}(u_k^{j+1})_n & \text{on } \left(\Gamma^{+}_{u,c,k-1}\right)^{j+1}, \\ 0 & \text{on } \left(\Gamma^{-}_{u,c,k-1}\right)^{j+1}. \end{cases} \quad (69)$$

Thus, we replace formulae (61)-(63) by equations (68) and (69). At the end of this section the complete algorithm is described.

Matrix factorization Due to the multiscale nature of the fictitious domain problem, the large thermal stresses and the implementation of the penalty term of the contact condition, the linear system of equations could not be solved by using iterative methods, so a direct one is applied. Since the computational domain grows with time far from the contact region and the stiffness matrix $\mathbf{K}$ changes at each contact iteration, in order to reduce the computational demands, we apply a partial factorization which let us recalculate only the submatrix corresponding to the contact nodes. Then, we propose to use:

- a mesh numbering such that the contact nodes correspond with the first ones;
- a factorization of the type $\mathbf{K} = \mathbf{U}\mathbf{D}\mathbf{U}^{\mathbf{T}}$, where $\mathbf{D}$ is a diagonal matrix and $\mathbf{U}$ is an upper triangular matrix with unitary diagonal;
- a storage by means of an upper skyline by rows; so, we storage the upper submatrix of $\mathbf{K}$ row by row from downwards to upwards and from the right to the left.

We apply a factorization row by row following the expressions

$$
\begin{aligned}
&D_{nn} = K_{nn},\\
&i = n-1, n-2, \ldots, 1\\
&\qquad U_{in} = \frac{K_{in}}{D_{nn}},\\
&\qquad\qquad K_{ij} - \sum_{l=j+1}^{n} U_{il} D_{ll} U_{jl}\\
&\qquad U_{ij} = \frac{}{D_{jj}}, \quad j = n-1, n-2, \ldots, i+1,\\
&\qquad D_{ii} = K_{ii} - \sum_{l=i+1}^{n} U_{il}^2 D_{ll},
\end{aligned}
$$

where $n = 3N_h(t)$ is the number of degrees of freedom at each time instant t. With this methodology, at each iteration we only recompute and factorize the first n_c rows of the matrix, n_c being the number of degrees of freedom on the contact boundary (see [13] and [77]).

Testing the algorithm. Test ($T2$) Here we check the Newton algorithm combined with the partial factorization strategy when they are applied to solve contact problems. For that purpose, in [13] we have solved an academic two-dimensional thermo-elastic test whose solution presents a gap between the slab and the rigid foundation, similar to the butt curl deformation in a real aluminium casting process. We have compared the efficiency of this algorithm with the SBM algorithm.

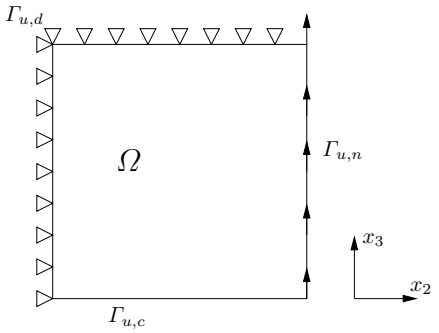

Fig. 12 Computational domain of Test ($T2$).

Let $(0, 200\text{s}]$ be the time interval of interest. We consider the cylindrical body whose axis is parallel to x_1-direction and whose section is the square of dimensions 0.5m×0.5m in the plane x_2x_3. We consider the plane strain assumption over the plane x_2x_3 and then its numerical simulation on the two-dimensional domain Ω shown in Figure 12. For the sake of simplicity, we

consider Ω independent of time. On $\partial\Omega$ we distinguish three disjoint and open parts:

$$\partial\Omega = \bar{\Gamma}_{u,d} \cup \bar{\Gamma}_{u,n} \cup \bar{\Gamma}_{u,c},$$

where

$$\bar{\Gamma}_{u,d} = \partial\Omega \cap ([x_2 = 0] \cup [x_3 = 0.5]), \bar{\Gamma}_{u,n} = \partial\Omega \cap [x_2 = 0.5],$$
$$\bar{\Gamma}_{u,c} = \partial\Omega \cap [x_3 = 0].$$

Let

$$T(t) = T_l + (100 - T_l)\frac{t}{200},\ t \in [0, 200] \tag{70}$$

be the temperature function and $T_l = 649°\text{C}$. Notice that the slab temperature is constant at each time instant and lower than T_l at $t > 0$.

In this test we assume that the material is thermo-elastic and we consider the elastic parameters $E = 1.e9\text{N/m}^2$, $\nu = 0.35$, which are independent of time and of temperature. We denote by λ and μ the corresponding Lamé coefficients. The coefficient of thermal expansion is given by expression (11), where the mass density function is (see El-Raghy *et al.* [40])

$$\rho(T) = \begin{cases} 2700 - 0.23T \text{ if } T \leq T_s, \\ 2360 \qquad\quad \text{if } T = T_l, \end{cases} \tag{71}$$

$T_s = 607°C$ being the solidus temperature. The values of $\rho(T)$ for $T \in (T_s, T_l)$ are approximated by linear interpolation. These data correspond to an aluminium alloy used in the numerical simulation of Section 5.

The problem to solve is

Test $(T2)$:

$$\left.\begin{aligned} -\text{Div}(\boldsymbol{\sigma}) = \mathbf{f} \text{ in } \Omega, \\ \mathbf{u} = \widehat{\mathbf{u}} \text{ on } \Gamma_{u,d}, \\ \boldsymbol{\sigma}\mathbf{n} = (0, 0, 3\mu h^2) \text{ on } \Gamma_{u,n}, \\ \boldsymbol{\sigma}_\tau = \mathbf{m},\ \sigma_n \leq 0,\ u_n \leq 0,\ \sigma_n u_n = 0 \text{ on } \Gamma_{u,c}, \\ \boldsymbol{\varepsilon}(\mathbf{u}) = \Lambda\boldsymbol{\sigma} + \displaystyle\int_{T_l}^{T} \alpha(r)\,dr\ \mathbf{I} \text{ in } \Omega, \\ \mathbf{u}(0) = \widehat{\mathbf{u}}(0),\ \ \boldsymbol{\sigma}(0) = \widehat{\boldsymbol{\sigma}}(0) \text{ in } \Omega, \end{aligned}\right\}$$

with

$$\mathbf{f}(\mathbf{x}, t) = \begin{cases} -3(\lambda + \mu)h^2\mathbf{e}_2 - 6\mu h x_3 \mathbf{e}_3, & \text{if } x_2 \leq \hat{x}_2(t), \\ -6\mu h \mathbf{e}_3, & \text{if } x_2 > \hat{x}_2(t), \end{cases}$$

$$\mathbf{m}(\mathbf{x}, t) = \begin{cases} -3h^2\mu x_3 \mathbf{e}_2, & \text{if } x_2 \leq \hat{x}_2(t), \\ -3h^2\mu \mathbf{e}_2, & \text{if } x_2 > \hat{x}_2(t), \end{cases}$$

$$\widehat{\mathbf{u}}\,(\mathbf{x}, t) = \frac{E}{2\mu}\left(\int_{T_l}^{T} \alpha(r)\,dr\right)(x_2\mathbf{e}_2 + x_3\mathbf{e}_3) + \begin{cases} h^3 x_3 \mathbf{e}_3, & \text{if } x_2 \leq \hat{x}_2(t), \\ h^3 \mathbf{e}_3, & \text{if } x_2 > \hat{x}_2(t), \end{cases}$$

$$\widehat{\boldsymbol{\sigma}}(\mathbf{x}, t) = -E\left(\int_{T_l}^{T} \alpha(r)\,dr\right)\mathbf{E}_1 + \begin{cases} \lambda h^3 \mathbf{I} + 2\mu h^3 \mathbf{E}_2 + 3\mu h^2 x_3 \mathbf{E}_3, & \text{if } x_2 \leq \hat{x}_2(t), \\ 3\mu h^2 \mathbf{E}_3, & \text{if } x_2 > \hat{x}_2(t), \end{cases}$$

where

$$\mathbf{E}_1 = \begin{pmatrix} 1\,0\,0 \\ 0\,0\,0 \\ 0\,0\,0 \end{pmatrix}, \mathbf{E}_2 = \begin{pmatrix} 0\,0\,0 \\ 0\,0\,0 \\ 0\,0\,1 \end{pmatrix}, \mathbf{E}_3 = \begin{pmatrix} 0\,0\,0 \\ 0\,0\,1 \\ 0\,1\,0 \end{pmatrix},$$

and

$$h(x_2, t) = x_2 - \hat{x}_2(t), \quad \hat{x}_2(t) = 0.4 - 1.e{-}3t.$$

The solution of Test $(T2)$ is $\mathbf{u} = \widehat{\mathbf{u}}$, $\boldsymbol{\sigma} = \widehat{\boldsymbol{\sigma}}$.

We use a uniform spatial mesh with 12800 triangles and 6561 vertices and for time discretization $\Delta t = 0.1$s. We initialize the contact multiplier by

$$p^0 = \begin{cases} 1, & \text{on } (\Gamma_{u,c}^+)^0, \\ 0, & \text{on } (\Gamma_{u,c}^-)^0. \end{cases}$$

Finally, we consider the following parameters:

– for the SBM algorithm:

$$\gamma_c = 0.5e9,\ \lambda_c = 1.e{-}9,\ \vartheta = 0.9;$$

– for the Newton algorithm:

$$\lambda_c = \frac{1}{\Delta t},\ \epsilon_c = 1.e{-}15,\ \vartheta = 0.9.$$

At time t^j, the stopping test on the contact multiplier p_k^j is

$$\begin{aligned} |p_k^j - p_{k-1}^j| < \tilde{\delta} \max\{\tilde{\delta}, |\, p_k^j|\},\ \forall C \in \mathcal{S}_h, \text{ and} \\ |p_k^j - G_{\lambda_c}(s_k^j)| < \tilde{\delta} \max\{\tilde{\delta}, |\, G_{\lambda_c}(s_k^j)|\},\ \forall C \in \mathcal{S}_h, \end{aligned}$$

where $\tilde{\delta}$ is a small parameter and $s_k^j = (u_k^j)_n + \lambda_c p_k^j$. Notice that, with this stopping test, if the multiplier is close to zero we perform an absolute test with $\tilde{\delta}^2$ and, in the other case, a relative test with $\tilde{\delta}$. In this case, we consider $\tilde{\delta} = 1.e{-}3$.

Figure 13 shows the displacements on the deformed configuration and the Von Mises norm of stresses at the last time step. In this test we compare the results obtained with the Newton algorithm with those obtained with the SBM one. The L^2 relative error at the last time step obtained with both algorithms is $3.957e-4$ in displacements and $7.452e-3$ in stresses. Table 4 gathers the obtained results, showing that with Newton algorithm the cpu-time decreases approximately 74% with respect to the SBM method and the number of iterations decreases 99%. These results show the good applicability of the Newton method for contact problems.

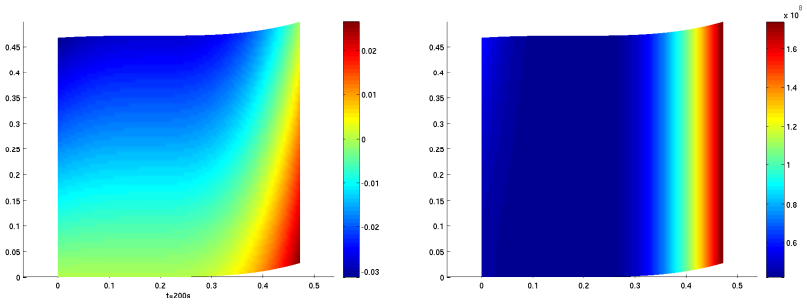

Fig. 13 Displacements on the deformed configuration and Von Mises norm at the last time step.

Table 4 Cpu-time and average number of iterations with $\Delta t = 0.1$s for contact Test ($T2$).

Method	SBM	Newton method
cpu-time (s)	17480.61	4615.30
iterations	258	3

4.3.2 Dealing with the nonlinear behaviour law

In this subsection, we improve the convergence of the viscoplastic multiplier in SBM algorithm. For this purpose, as in Subsection 4.2.2, the thermo-elastic-viscoplastic law is discretized in time by using an implicit Euler scheme and Lemmas 2 and 3 are applied with $\gamma_p = 0$. Therefore, the viscoplastic multiplier $\mathbf{q}^{j+1}$, defined in Ω_s^{j+1}, verifies (see (53)):

$$\mathbf{q}^{j+1} = (D_\sigma \Phi_q)_{\lambda_p} \left(\left(\boldsymbol{\sigma}^{j+1}\right)^D + \lambda_p \mathbf{q}^{j+1}, T^{j+1} \right), \tag{72}$$

being

$$(D_\sigma \Phi_q)_{\lambda_p} (\boldsymbol{\zeta}, T) = \frac{1}{\lambda_p} \left(1 - \frac{1}{\eta} \right) \boldsymbol{\zeta},$$

and $\eta = \eta(\boldsymbol{\zeta}, T)$ the unique root in the interval $[1, +\infty)$ of the equation

$$\eta^{q-1} - \eta^{q-2} - \lambda_p \kappa(T) |\boldsymbol{\zeta}|^{q-2} = 0. \tag{73}$$

Assuming that the stress tensor is known, in [5] we linearize equation (72) to obtain an approximation of the viscoplastic multiplier, and we prove the following lemmas.

Lemma 6 *Given any $\boldsymbol{\sigma} \in \mathcal{S}_3$, $T \in \mathbb{R}$ and $\lambda_p > 1$, the fixed point $\mathbf{q} \in \mathcal{S}_3$ of the equation*

$$\mathbf{q} = (D_\sigma \Phi_q)_{\lambda_p} \left(\boldsymbol{\sigma}^D + \lambda_p \mathbf{q}, T \right)$$

can be approximated by

$$\begin{aligned} \mathbf{q} \cong\, & (D_\sigma \Phi_q)_{\lambda_p} \left(\boldsymbol{\sigma}^D + \lambda_p \hat{\mathbf{q}}, T \right) + \left(1 - \frac{1}{\eta} \right) (\mathbf{q} - \hat{\mathbf{q}}) \\ & + \bar{\eta} \left(\left(\boldsymbol{\sigma}^D + \lambda_p \hat{\mathbf{q}} \right) : (\mathbf{q} - \hat{\mathbf{q}}) \right) \left(\boldsymbol{\sigma}^D + \lambda_p \hat{\mathbf{q}} \right), \end{aligned}$$

for $\hat{\mathbf{q}} \in \mathcal{S}_3$ *close enough to* $\mathbf{q}$ *and provided that* $\boldsymbol{\sigma}^D + \lambda_p \hat{\mathbf{q}} \neq \mathbf{0}$. *Here* $\eta = \eta\left(\boldsymbol{\sigma}^D + \lambda_p \hat{\mathbf{q}}, T\right)$ *is given by equation (73), and* $\bar{\eta}$ *is defined by the expression*

$$\bar{\eta} = \frac{(q-2)(\eta-1)}{\eta\left((q-1)\eta-(q-2)\right)\left|\boldsymbol{\sigma}^D + \lambda_p \hat{\mathbf{q}}\right|^2}.$$

The order of this approximation is $O\left(|\mathbf{q}-\hat{\mathbf{q}}|^2\right)$.

The fixed point of (72) can be explicitly computed thanks to the following lemma.

Lemma 7 *At each time step* t^{j+1}, $j = 0, \ldots, N-1$, *and at each iteration* $k > 0$, *the fixed point* $\mathbf{q}_k^{j+1}$ *of equation (72) can be computed using the recurrence formula*

$$\mathbf{q}_k^{j+1} = \begin{cases} \mathbf{0}, & \text{if } \varkappa_k^{j+1} = \mathbf{0}, \\ \frac{\left(\eta_k^{j+1}-1\right)}{\lambda_p}\left(\left(\boldsymbol{\sigma}_k^{j+1}\right)^D + \left(\eta_k^{j+1}-1\right)\frac{q-2}{\eta_k^{j+1}}\varkappa_k^{j+1}\right) & \\ \quad -\left(\eta_k^{j+1}-1\right)\frac{q-2}{|\varkappa_k^{j+1}|^2}\left(\mathbf{q}_{k-1}^{j+1} : \varkappa_k^{j+1}\right)\varkappa_k^{j+1}, & \text{if } \varkappa_k^{j+1} \neq \mathbf{0}, \end{cases} \tag{74}$$

in Ω_s^{j+1}, *where* $\varkappa_k^{j+1}$ *is given by*

$$\varkappa_k^{j+1} = \left(\boldsymbol{\sigma}_k^{j+1}\right)^D + \lambda_p\, \mathbf{q}_{k-1}^{j+1},$$

and $\eta_k^{j+1} = \eta\left(\varkappa_k^{j+1}, T^{j+1}\right)$.

Adimensionalization technique Due to the large thermal stresses that appear in the slab during aluminium casting, sometimes convergence is not achieved when using the Newton algorithm described above to approximate the viscoplastic multiplier. To solve this, in [5] we proposed to employ an adimensionalization technique on the stresses. This technique consists of choosing a reference stress and introducing new nondimensional unknowns in order to transfer the magnitude of the stresses to the coefficients of the behaviour law (46) to solve a similar problem for these new unknowns.

Testing the algorithm. Test $(T3)$ Here we check the Newton algorithm combined with the adimensionalization technique when they are applied to solve elastic-viscoplastic problems. In this test, large gradients of the stress tensor appear – from null value to 10^8–, a similar situation like in casting processes, when a part of the material is recently solidified.

Let $(0, 0.5\text{s}]$ be the time interval of interest. We consider the cylindrical body detailed in Test $(T2)$, also under the plane strain assumption. On the boundary of its cross section Ω, we distinguish two disjoint and open parts, $\partial\Omega = \bar{\Gamma}_{u,d} \cup \bar{\Gamma}_{u,n}$, where

$$\bar{\Gamma}_{u,d} = \partial\Omega \cap \left([x_2 = 0] \cup [x_3 = 0]\right), \ \bar{\Gamma}_{u,n} = \partial\Omega \cap \left([x_2 = 0.5] \cup [x_3 = 0.5]\right).$$

We consider that Ω is an already solidified block with constant temperature. Then, there are not thermal stresses and the material parameters corresponding to the constitutive law, independent of the temperature, are taken as:

$$E = 1.e9\mathrm{N/m}^2,\ \nu = 0.35,\ \theta_0 = 1.953125e{-}39\mathrm{m}^2/(\mathrm{sN}),\ q = 6.$$

Then, the problem to solve is

Test $(T3)$:
Find $\mathbf{u}$ and $\boldsymbol{\sigma}$ such that

$$\left.\begin{aligned} \mathrm{Div}(\boldsymbol{\sigma}) &= \mathbf{0} \text{ in } \Omega, \\ \mathbf{u} &= h\,(t)\,(0, x_2, -x_3) \text{ on } \Gamma_{u,d}, \\ \boldsymbol{\sigma}\mathbf{n} &= \mathbf{g} \text{ on } \Gamma_{u,n}, \\ \boldsymbol{\varepsilon}(\dot{\mathbf{u}}) &= \Lambda\dot{\boldsymbol{\sigma}} + \theta_0 \mid \boldsymbol{\sigma}^D \mid^{q-2} \boldsymbol{\sigma}^D \text{ in } \Omega, \\ \mathbf{u}(x,0) &= \mathbf{0},\ \ \boldsymbol{\sigma}(x,0) = \mathbf{0} \text{ in } \Omega, \end{aligned}\right\} \tag{75}$$

with $h\,(t) = 1.e8\dfrac{1+\nu}{E}t + \dfrac{2}{3}1.e40\,\theta_0 t^6$ and

$$\mathbf{g}(x,t) = \begin{cases} 1.e8\,t\mathbf{n}, & \text{on } \Gamma_{u,n} \cap [x_2 = 0.5], \\ -1.e8\,t\mathbf{n}, & \text{on } \Gamma_{u,n} \cap [x_3 = 0.5]. \end{cases}$$

The solution of Test $(T3)$ is readily verifiable

$$\mathbf{u}(x,t) = h\,(t)\,(0, x_2, -x_3)\,,\ \boldsymbol{\sigma}(x,t) = 1.e8 \begin{pmatrix} 0 & 0 & 0 \\ 0 & t & 0 \\ 0 & 0 & -t \end{pmatrix}.$$

To solve this test we use a uniform spatial mesh with 800 elements and 441 nodes, corresponding to a discretization parameter $\Delta x = 0.025$m and for time discretization we use a small time step $\Delta t = 1.e-5$s since the solution is nonlinear in time. We compute the initial viscoplastic multiplier as

$$\mathbf{q}^0 = \kappa(T^0)\left|(\boldsymbol{\sigma}^0)^D\right|^{q-2}(\boldsymbol{\sigma}^0)^D = \mathbf{0},$$

and we consider the following parameters:

- for the SBM algorithm:

$$\gamma_p = 1.e{-}6,\ \lambda_p = 0.5e6,\ \vartheta = 0.9;$$

- for the Newton algorithm:

$$\lambda_p = 1,\ \vartheta = 0.9.$$

At each time step t^j, a stopping test at each component of the viscoplastic multiplier is performed, analogously to that of contact multiplier in Test $(T2)$.

The results obtained with the Newton method together with the adimensionalization technique improved those obtained with SBM algorithm, with a 85% decrease in the cpu-time and a 95% in the average number of iterations (see Table 5).

Table 5 Comparison of cpu-time and average number of iterations with $\Delta t = 1.e-5$ for elastic-viscoplastic Test ($T3$).

Method	SBM	Newton method
cpu-time (s)	18790.2	2744.0
iterations	57	3
$\mathbf{u}$ error	$2.622e-5$	$2.621e-5$
$\boldsymbol{\sigma}$ error	$1.245e-5$	$1.244e-5$

4.3.3 NBM algorithm

Here, we summarize the Bermúdez-Moreno algorithm combined with Newton methods proposed in Subsections 4.3.1 and 4.3.2 to approximate both viscoplastic and contact multipliers when solving the casting problem. In the following, this algorithm is denoted by NBM algorithm.

NBM1 Equal to SBM1.

NBM2 Then, for $j \geq 0$, ($\mathbf{u}^j$, $\boldsymbol{\sigma}^j$, $\mathbf{q}^j$, p^j) known at time t^j, we determine ($\mathbf{u}^{j+1}, \boldsymbol{\sigma}^{j+1}$, $\mathbf{q}^{j+1}$, p^{j+1}) at time t^{j+1} by using the following iterative algorithm:

(a) Equal to SBM2(a).

(b) With $\mathbf{q}_{k-1}^{j+1}, p_{k-1}^{j+1}$ known, compute $(\mathbf{u}_k^{j+1}, p_k^{j+1})$ with $k \geq 1$ in two steps:

(i) Solve the variational equality

$$\int_{\Omega_s^{j+1}} \left(\Lambda(T^{j+1})\right)^{-1} \boldsymbol{\varepsilon}(\mathbf{u}_k^{j+1}) : \boldsymbol{\varepsilon}(\mathbf{v}) dx + \int_{\Omega_l^{j+1}} \Lambda_l^{-1} \boldsymbol{\varepsilon}(\mathbf{u}_k^{j+1}) : \boldsymbol{\varepsilon}(\mathbf{v}) dx +$$
$$\frac{1}{\epsilon_c} \int_{(\Gamma^+_{u,c,k-1})^{j+1}} \left(u_k^{j+1}\right)_n v_n d\gamma = \int_{\Omega^{j+1}} \mathbf{f}^{j+1} \cdot \mathbf{v} dx +$$
$$\int_{\Omega_s^{j+1}} \left(\Lambda(T^{j+1})\right)^{-1} \left(\Delta t \mathbf{q}_{k-1}^{j+1} - \mathbf{F}^j\right) : \boldsymbol{\varepsilon}(\mathbf{v}) dx, \; \forall \mathbf{v} \in \mathbf{U}_h(t^{j+1}),$$

where

$$\mathbf{F}^j = \Lambda(T^j)\boldsymbol{\sigma}^j - \boldsymbol{\varepsilon}(\mathbf{u}^j) - \alpha(T^{j+1})(T^{j+1} - T^j)\mathbf{I} \text{ in } \Omega_s^{j+1}.$$

(ii) Update the contact multiplier p_k^{j+1} with expression (69) and the effective contact boundary with (66).

(c) The stress tensor is updated analogously to SBM2(c) with $\gamma_p = 0$.

(d) The updated viscoplastic multiplier is given by equation (74).

Remark 6 Notice that, in NBM algorithm, the automorphism $\mathcal{V}(T^{j+1})$ is replaced by $\Lambda^{-1}(T^{j+1})$.

Figure 14 shows a flowchart of NBM algorithm. After initializing variables (Step 1 in Figure 14), a time step loop is carried out. In this loop, at the $j+1$ time step, the displacement vector $\mathbf{u}^{j+1}$ is computed by constructing the fixed

stiffness matrix (Step 2) and solving iteratively NBM2(b)-NBM2(d) (Steps 5-10), where the variable stiffness matrix is constructed at each iteration (Step 6).

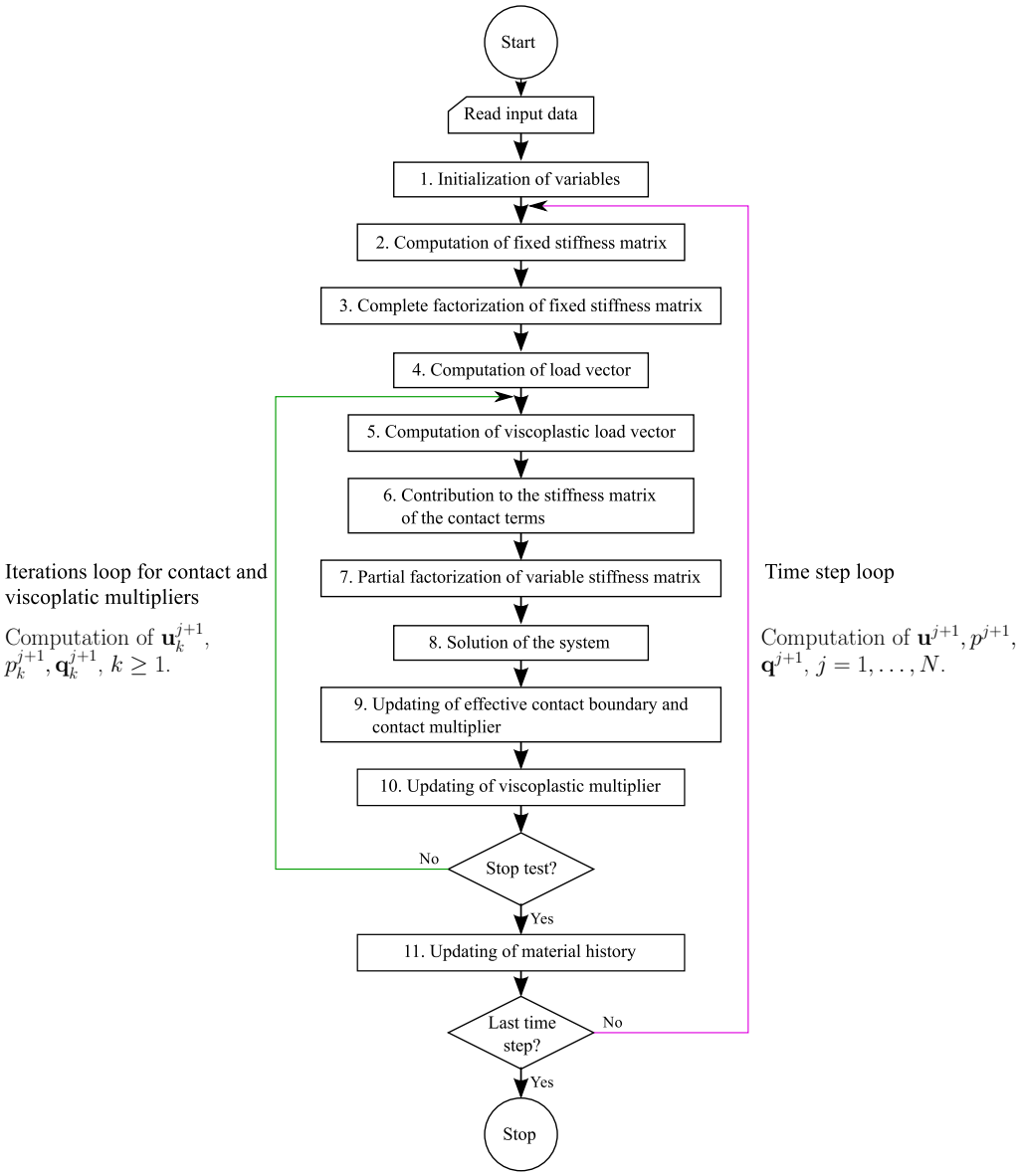

Fig. 14 Flowchart for NBM algorithm.

4.3.4 Improvements of NBM algorithm

Newton method is known to be an efficient method, but, unfortunately, in time-dependent problems, it is necessary to use a very small time step discretization in order to have a good initial approach. Since the time interval of interest to reproduce the butt curl deformation is about 150 s, if we want to apply NBM algorithm we should be able to increase the time step. To overcome this difficulty, in [5] we proposed to use an optimization technique on the time step in such a way that, given an initial fixed Δt, if convergence is not achieved, the time step is automatically reduced until the algorithm converges. When the convergence is stabilized, the time step is again automatically increased. Furthermore, to stabilize the Newton method we also employed an Armijo rule on the computation of the viscoplastic multiplier (see Bertsekas [24]).

Testing the algorithm. Test $(T4)$ In order to check the NBM algorithm combined with the above improvements, we consider a modification of Test $(T3)$ to also include a Signorini contact condition with a rigid obstacle. To do that, in Test $(T4)$, $\Gamma_{u,d}$ is reduced to $\bar{\Gamma}_{u,d} = \partial\Omega \cap [x_2 = 0]$, considering a new part of the boundary, $\Gamma_{u,c}$, defined by (see Figure 15):

$$\bar{\Gamma}_{u,c} = \partial\Omega \cap [x_3 = 0].$$

Test $(T4)$ keeps all the equations and data of Test $(T3)$ and it also includes the Signorini contact condition on $\Gamma_{u,c}$; the solutions of both tests are equal.

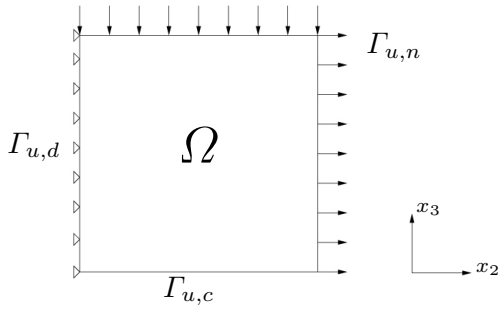

Fig. 15 Computational domain of Test $(T3)$.

We initialize the viscoplastic and contact multipliers by $\mathbf{q}^0 = \mathbf{0}$, $p^0 = 1.e{-}15$, and we consider the following parameters:

– for the SBM algorithm:

$$\gamma_c = 0.5e12,\ \lambda_c = 1.e{-}12,$$
$$\gamma_p = 1.{-}6,\ \lambda_p = 0.5e6,$$
$$\vartheta = 0.9;$$

– for the NBM algorithm:

$$\lambda_c = \lambda_p = 1,\ \epsilon_c = 1.e{-}50,\ \vartheta = 0.9.$$

Table 6 Comparison of cpu-time and average number of iterations with $\Delta t = 1.e{-}5$ for Test ($T4$).

Method	SBM	NBM
cpu-time (s)	25256.8	5365.2
iterations	69	3
$\mathbf{u}$ error	2.918×10^{-5}	2.917×10^{-5}
$\boldsymbol{\sigma}$ error	1.345×10^{-5}	1.345×10^{-5}

Table 6 shows the obtained results with the SBM and NBM algorithms when considering a small time step. Notice that with the NBM algorithm the average number of iterations decreases approximately 95% and the cpu-time 85% with respect to the SBM algorithm.

Aiming to simulate the butt curl simulation, an increase in the time step is necessary. If we consider $\Delta t = 0.0625$, NBM algorithm does not converge except that we use the automatic optimization of the time step described above. In this case, the time step is reduced from 0.0625 s to 0.015625 s. Table 7 shows the obtained results with SBM and NBM algorithms; the NBM algorithm obtains smaller displacement and stress errors than the SBM one and the reduction in cpu-time is 48% and in the average number of iterations 93%.

Table 7 Comparison of cpu-time and average number of iterations with $\Delta t = 0.0625$ for Test ($T4$).

Method	SBM	NBM
cpu-time (s)	6.58	3.39
iterations	254	18
$\mathbf{u}$ error	$2.66e{-}1$	$7.30e{-}2$
$\boldsymbol{\sigma}$ error	$1.63e{-}1$	$2.70e{-}2$

4.4 Bermúdez-Moreno algorithm with variable parameters

In this Section we propose to take advantage of the robustness of the SBM algorithm and to improve it with the methodology presented in Parés *et al.* [74] and Gallardo *et al.* [45], who introduced a procedure to automatically compute the optimal parameters of the algorithm. In the latter paper, the authors introduced a generalized Yosida regularization and they presented a generalization of the Bermúdez-Moreno algorithm that allows the use of very general

operators as parameters. Moreover, as a particular case, they analyzed the use of scalar and matrix-valued parameters, proving that the optimal choice of the parameter γ_p is a matrix-valued function. An application of this generalized algorithm with scalar parameters in one-dimensional problems can be seen in Arregui *et al.* [2].

Since our viscoplastic law varies greatly depending on whether the element is recently solidified or not, the SBM algorithm strongly depends on the choice of the two constant parameters λ_p, γ_p involved to approach the viscoplastic multiplier (see equation (56)). Thus, taking into account the complexity of the real problem, we propose to replace the constant parameters by scalar functions depending on time and space (see [14]). We will see in Section 5 that, although in Gallardo *et al.* [45] this choice did not give good results in some academic cases, in casting processes the convergence improvement is considerable. This fact is due to the great variation of viscoplastic behaviour from one element to another and from one time step to another, which explains the poor convergence results when considering γ_p constant.

In this section we restrict ourselves to the associated two-dimensional problem under the plane strain assumption on the symmetry plane $[x_1 = 0]$. As we have announced, we consider again SBM algorithm and we assume there that γ_p, λ_p are functions from $\Omega \times (0, t_f)$ to $\mathbb{R}$. From Lemma 3, at each time step t^j, given γ_p^j, λ_p^j, the viscoplastic multiplier verifies

$$\mathbf{q}^j = (D_\sigma \Phi_q)_{\lambda_p^j}^{\gamma_p^j} \left(\left(\boldsymbol{\sigma}^j\right)^D + \lambda_p^j \mathbf{q}^j, T^j \right), \tag{76}$$

where $\boldsymbol{\sigma}^j$ is obtained from equation (54) at the time step t^j. The main question is to determine a suitable technique to compute the value of parameters γ_p^j, λ_p^j from the solution obtained at the time step t^j. Taking into account that the optimal parameters to convergence verify $\lambda_p^j \gamma_p^j = 1/2$ (see Bermúdez and Moreno [19] or Parés *et al.* [73]), the problem is reduced to compute one of them, for example, γ_p^j.

Taking into account that Norton-Hoff's law (27) only involves the deviatoric part of the stress tensor, in this study we consider for each element $K \in \mathcal{T}_h(t^j)$ the space of matrices with null trace under the plane strain assumption:

$$\mathcal{S}^D = \{\boldsymbol{\tau} = (\tau_{ij}) \in \mathcal{M}_{3\times 3}(\mathbb{R}); \tau_{ij} = \tau_{ji}, \tau_{12} = \tau_{13} = 0, \tau_{11} = -(\tau_{22} + \tau_{33})\}.$$

We introduce the following notation:

– H denotes the derivative application of the viscoplastic function Φ_q defined in expression (21):

$$\begin{aligned} H : \mathcal{S}^D &\longrightarrow \mathcal{S}^D \\ \boldsymbol{\tau} &\longrightarrow H(\boldsymbol{\tau}) = \kappa |\boldsymbol{\tau}|^{q-2} \boldsymbol{\tau}. \end{aligned}$$

Notice that the dependence of Φ_q on the temperature is omitted since, in practice, we consider that the temperature is constant at each element of the mesh.

– Given $\boldsymbol{\zeta} \in \mathcal{S}^D$ and $\mathbf{q} = H^{\gamma_p}(\boldsymbol{\zeta}) \in \mathcal{S}^D$, we denote $\tilde{H}^{\gamma_p}_{1/(2\gamma_p)}$ as

$$\tilde{H}^{\gamma_p}_{1/(2\gamma_p)}(\mathbf{q}) = H^{\gamma_p}_{1/(2\gamma_p)}\left(\boldsymbol{\zeta} + \frac{1}{2\gamma_p}\mathbf{q}\right),$$

where $H^{\gamma_p}_{1/(2\gamma_p)}$ is the regularized Yosida of the perturbed operator $H^{\gamma_p} = H - \gamma_p \mathbf{I}$.

With this notation, if $\lambda_p^j \gamma_p^j = 1/2$, the viscoplastic multiplier $\mathbf{q}^j|_K$, given by expression (76), can be rewritten at each time step t^j and over each element K as:

$$\mathbf{q}^j|_K = H^{\gamma_p^j|_K}_{1/(2\gamma_p^j|_K)}\left(\left(\boldsymbol{\sigma}^j|_K\right)^D + \frac{1}{2\gamma_p^j|_K}\mathbf{q}^j|_K\right) = \tilde{H}^{\gamma_p^j|_K}_{1/(2\gamma_p^j|_K)}\left(\mathbf{q}^j|_K\right).$$

Hence, $\mathbf{q}^j|_K$ can be obtained as the fixed point of $\tilde{H}^{\gamma_p^j|_K}_{1/(2\gamma_p^j|_K)}$ at each time step and over each element of the mesh. The strategy proposed in Gallardo *et al.* [45] consists of finding at each element K and at each time step t^j the critical points of $\tilde{H}^{\gamma_p^j|_K}_{1/(2\gamma_p^j|_K)}$ or, equivalently, finding a parameter $\gamma_p^j|_K$ verifying

$$D\tilde{H}^{\gamma_p^j|_K}_{1/(2\gamma_p^j|_K)}(\mathbf{q}^j|_K) = \mathbf{0}.$$

For that purpose, in the following lemma its spectral radius is minimized (see [14]).

Lemma 8 *Let assume that* $DH\left(\left(\boldsymbol{\sigma}^j\right)^D\right)$ *is positive definite and consider that* $0 < \omega_1^j \leq \omega_2^j \leq \omega_3^j$ *are its eigenvalues. Then,*

$$\frac{\omega_i^j - \gamma_p}{\omega_i^j + \gamma_p}$$

are the eigenvalues of $D\tilde{H}^{\gamma_p}_{1/(2\gamma_p)}(\mathbf{q}^j)$ *for* $\mathbf{q}^j = H^{\gamma_p}\left(\left(\boldsymbol{\sigma}^j\right)^D\right)$ *and its spectral radius is*

$$\rho^j_{\gamma_p} = \max_{i=1,2,3}\left|\frac{\omega_i^j - \gamma_p}{\omega_i^j + \gamma_p}\right|.$$

In [14] we have also proved the following theorem, which gives the optimal values for parameters γ_p^j, λ_p^j:

Theorem 2 *The optimal choice of parameters for the viscoplastic multiplier* $\mathbf{q}^j|_K$ *at each time step* t^j *and over each element* K *of the mesh is*

$$\gamma_p^j|_K = \sqrt{\omega_1^j|_K\, \omega_3^j|_K}, \quad \lambda_p^j|_K = \frac{1}{2\gamma_p^j|_K}, \tag{77}$$

where $\omega_1^j|_K$ *and* $\omega_3^j|_K$*, eigenvalues of* $DH\left(\left(\boldsymbol{\sigma}^j|_K\right)^D\right)$*, are given by*

$$\omega_1^j|_K = B^j|_K, \quad \omega_3^j|_K = B^j|_K + \frac{2}{3}A^j|_K \left(\left(\sigma^j|_K\right)^D\right)_{eq}^2,$$

with

$$A^j|_K = \kappa(T^j|_K)(q-2)\left|(\boldsymbol{\sigma}^j|_K)^D\right|^{q-4},$$
$$B^j|_K = \kappa(T^j|_K)\left|(\boldsymbol{\sigma}^j|_K)^D\right|^{q-2},$$

and τ_{eq} *being the Von Mises equivalent stress defined by*

$$\tau_{eq} = \sqrt{\frac{3}{2}\boldsymbol{\tau} : \boldsymbol{\tau}}, \quad \boldsymbol{\tau} \in \mathcal{S}^D.$$

4.4.1 VNBM algorithm

In order to overcome the poor convergence of the SBM algorithm in the butt curl simulation of aluminium casting processes, we propose to combine the Newton algorithm for the contact nonlinearity introduced in Subsection 4.3.1, with the standard Bermúdez-Moreno algorithm with variable parameters for the viscoplastic nonlinearity presented in Section 4.4. In the following, this algorithm is denoted by VNBM algorithm. In practice, to avoid the factorization of the whole stiffness matrix, parameters γ_p and λ_p are updated only once when starting a new time step, after the stress tensor is computed on the previous time step.

VNBM1 Equal to SBM1.

VNBM2 Then, for $j \geq 0$, $(\mathbf{u}^j,\ \boldsymbol{\sigma}^j,\ \mathbf{q}^j,\ \gamma_p^j,\ p^j)$ known at time t^j, we determine $(\mathbf{u}^{j+1}, \boldsymbol{\sigma}^{j+1},\ \mathbf{q}^{j+1},\ \gamma_p^{j+1},\ p^{j+1})$ at time t^{j+1} by using the following iterative algorithm:

(a) Equal to SBM2(a).

(b) With $\mathbf{q}_{k-1}^{j+1}, p_{k-1}^{j+1}$ known, compute $(\mathbf{u}_k^{j+1}, p_k^{j+1})$ with $k \geq 1$ in two steps:
(i) Solve the variational equality

$$\int_{\Omega_s^{j+1}} \mathcal{V}(T^{j+1}) \left[\boldsymbol{\varepsilon}(\mathbf{u}_k^{j+1}) + \frac{\Delta t \gamma_p^j s^{j+1}}{3}\mathrm{tr}(\boldsymbol{\varepsilon}(\mathbf{u}_k^{j+1}))\mathbf{I}\right] : \boldsymbol{\varepsilon}(\mathbf{v})dx +$$
$$\int_{\Omega_l^{j+1}} \Lambda_l^{-1}\boldsymbol{\varepsilon}(\mathbf{u}_k^{j+1}) : \boldsymbol{\varepsilon}(\mathbf{v})dx + \frac{1}{\epsilon_c}\int_{(\Gamma_{u,c,k-1}^+)^{j+1}} \left(u_k^{j+1}\right)_n v_n d\gamma =$$
$$\int_{\Omega_s^{j+1}} \left[\mathcal{V}(T^{j+1})\Delta t \mathbf{q}_{k-1}^{j+1}\right] : \boldsymbol{\varepsilon}(\mathbf{v})dx - \int_{\Omega_s^{j+1}} \left[\mathcal{V}(T^{j+1})\mathbf{F}^j\right] : \boldsymbol{\varepsilon}(\mathbf{v})dx +$$
$$\int_{\Omega^{j+1}} \mathbf{f}^{j+1} \cdot \mathbf{v}dx \ \forall \mathbf{v} \in \mathbf{U}_h(t^{j+1}),$$

where $\mathbf{F}^j$ is given by formula (55) for $\gamma_p = \gamma_p^j$.

(ii) The contact multiplier is updated equal to NBM2(ii).

(c) The updated stress tensor is defined analogously to SBM2(c) with $\gamma_p = \gamma_p^j$.

(d) The updated viscoplastic multiplier is defined analogously to SBM2(d) with $\gamma_p = \gamma_p^j$ and $\lambda_p = \dfrac{1}{2\gamma_p^j}$.

(e) Once the convergence is achieved, the updated parameter γ_p^{j+1} and λ_p^{j+1} are given by expressions in (77) with a lag to the previous time step:.

The flowchart of VNBM algorithm is analogous to that in Figure 14, taking into account that, once the convergence is achieved at each time step, it is necessary to compute the value of parameter γ_p for the next time step.

Testing the VNBM algorithm In order to check the VNBM algorithm, as in Subsection 4.3.4, we consider again Test ($T4$). The parameters for VNBM algorithm are:

$$\lambda_c = 1,\ \epsilon_c = 1.e{-}50,\ \gamma_p^0 = 0.1,\ \vartheta = 0.9.$$

Table 8 shows a comparison between the three main algorithms presented in this paper. The reduction in cpu-time of the NBM algorithm with respect to the SBM is 48% and the reduction in iterations is 92%. From these results we can state that NBM method introduced in Subsection 4.3.3 is a good method to solve mechanical problems with elastic-viscoplastic laws of Maxwell-Norton type and with a Signorini contact condition. Nevertheless, when using this method to simulate real casting processes, convergence of NBM method slows down dramatically.

Otherwise, although the NBM algorithm obtain better results for this test, the reduction in cpu-time (40%) and iterations (83%) of the VNBM algorithm with respect to the SBM is considerable. In addition, if we take into account that the Newton method has convergence problems in the recently solidified elements, due to the discontinuity of the viscoplastic stresses on the phase change, we can conclude that the VNBM algorithm is a very good alternative for the butt curl simulation of castings as we will see in the next section.

Table 8 Comparison of cpu-time and average number of iterations for elastic-viscoplastic test with contact.

Method	SBM	NBM	NVBM
cpu-time (s)	6.58	3.39	3.92
iterations	254	18	43
$\mathbf{u}$ error	$2.66e{-}1$	$7.30e{-}2$	$2.03e{-}1$
$\boldsymbol{\sigma}$ error	$1.63e{-}1$	$2.70e{-}2$	$8.40e{-}2$

5 Numerical results of an aluminium alloy casting process

In this section we present the results obtained in the numerical simulation of a real casting process. Real data have been provided by ALCOA-INESPAL, A Coruña, Spain. Firstly, we present the numerical results obtained with the SBM algorithm in the three-dimensional simulation of the process using the weak formulation ($EVMP$). We compare these results with the experimental ones obtained in plant. Secondly, due to that the start phase simulation is the most cpu-time consumption, with a considerable amount, we restrict ourselves to the two-dimensional case and we compare the results obtained with the three algorithms –SBM, NBM and VNBM– presented in this paper for this start phase. The objective is to provide real-time response to the engineer in plant and to show a good agreement between two and three-dimensional simulations.

The parameters to characterize the thermo-elastic-viscoplastic law of aluminium alloy (see equation (27)) have been introduced in our previous works [7–9] after carrying out a complete bibliographic search in the engineering literature (see El-Raghy *et al.* [40], Hatch [51], Lemaitre and Chaboche [61] or Wong and Jonas [85]). The data and parameters considered to carry out the casting problem simulations are the following:

- Volume forces: Equal to those considered in Test ($T2$) with $T_s = 620°\text{C}$.
- Elastic law: Values for Young's modulus, E, and Poisson's coefficient, ν, depending on temperature are obtained from Table 9 by linear interpolation.

Table 9 Elastic law parameters.

$T(°\text{C})$	$E(10^9\text{N/m}^2)$	ν
126.9	67	0.3134
326.9	58	0.3448
526.9	40	0.45

- Viscoplastic law: The viscoplastic parameter $\kappa(T)$ is computed from relations (16) and (20), and from the data of Table 10.

Table 10 Viscoplastic law parameters.

$\lambda_r(\text{N/sm}^2)$	$k(10^6\text{N/m}^2)$	$G(\text{Kcal/mol})$	q
$4.0e12$	15.72	37.3	6

- Thermal law: The coefficient of thermal expansion $\alpha(T)$, which includes volume changes due to phase transformations, is computed from the density function following equation (11).

– In practice, to impose the metallostatic pressure we consider in equation (38) that $\delta = 2$, $\beta = 1$, $\epsilon = 1.e{-}3$, $\overline{\lambda} = \lambda(T_l)$ and $\overline{\mu} = \mu(T_l)$, that is:

$$\bar{\lambda} = 1.2414e11,\ \bar{\mu} = 1.3793e10.$$

5.1 Numerical results for the three-dimensional simulation of the start and stationary stages

In [8] some results for the start and stationary stages of the above DC casting process were presented by using the SBM algorithm and a validation with experimental results were carried out.

Figure 16 shows the mesh of the computational domain at the start stage of the casting process with 7182 elements and 1600 nodes. Experimental measurements were made at a point near the bottom of the corner.

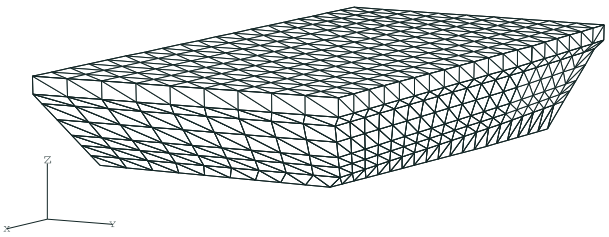

Fig. 16 Initial mesh of the slab used for the start stage.

Figure 17 (left) shows the numerical butt curl at time $t = 140$ s. The numerical vertical displacement of the test point marked in the figure at $t = 250$ s was 0.035 m and the experimental value 0.038 m. The numerical time dependence of the displacement modulus for this point is also shown in this graphic on the right.

In order to simulate the stationary stage, several factors must be taken into account: the growth of the domain with time and the variation of the region with the sharpest temperature gradients, which is always near the top and outer faces of the slab. So, the entire undeformed reference mesh is reconstructed at each time step; the new mesh being bigger than the previous one by an amount corresponding to the metal poured during the time step, and finest-grained where the temperature gradients are steepest. Figure 18 (left) shows the reference mesh obtained with this methodology at $t = 1000$ s with $\Delta t = 10$ s, which has 38016 elements and 7548 nodes. Saint-Venant principle, corroborated by two-dimensional simulations (see [8]), shows that the butt curl has no influence on the cross-sectional deformation caused by contraction of the lateral faces. Due to this, we decided that for the stationary stage the Signorini contact condition could be replaced by a simple constraint maintaining the butt surface in contact with the bottom block. Figure 18 (right) shows the contraction suffered by the lateral faces of the slab after 1000s of casting.

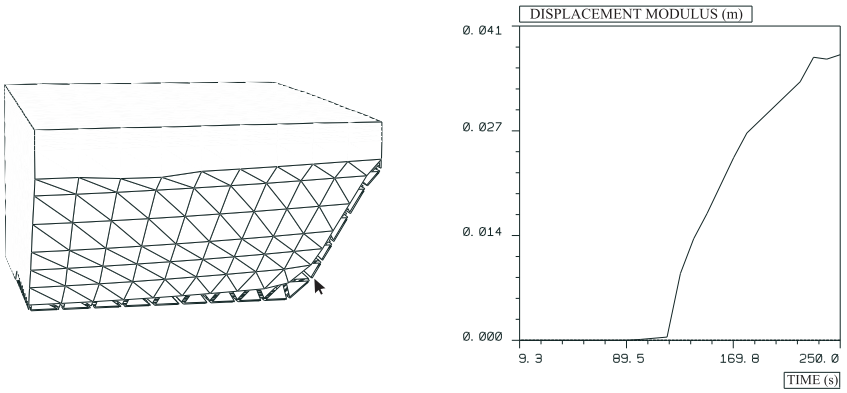

Fig. 17 Butt curl deformation after 140 s of casting. The arrow shows the point where experimental results were taken; at this point the time evolution of butt curl is shown in the graphic on the right.

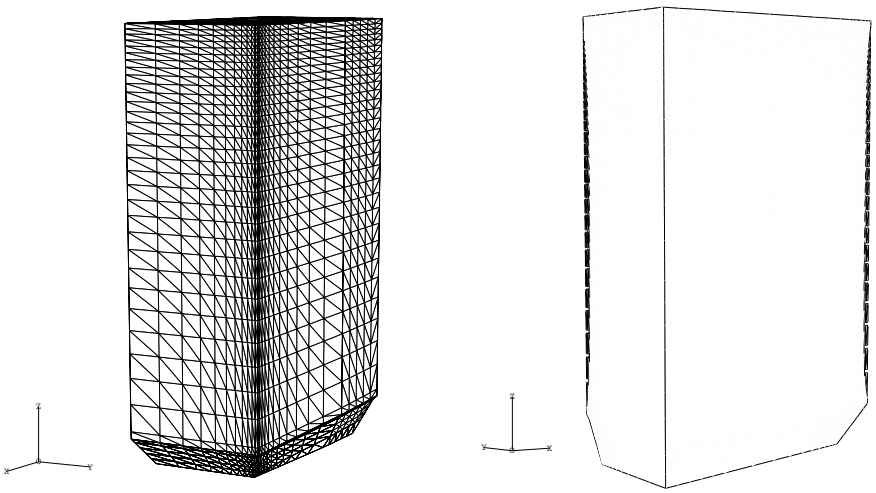

Fig. 18 Three-dimensional mesh of the slab –on the left– and contraction of the lateral faces –on the right– after 1000 s of casting.

Figure 19 shows the deformation obtained for a cross-section about halfway up the slab after 1000 s and compares the numerical slab profile in three different cross-sections with the collar geometry and the desired flat geometry, illustrating how contraction increases with time. In a cross-section near the butt, which changes negligibly after 1000 s, the calculated half-width in the y direction at the point where experimental measurements were made was 0.280 m, which compares well with the measured final value of 0.277 m.

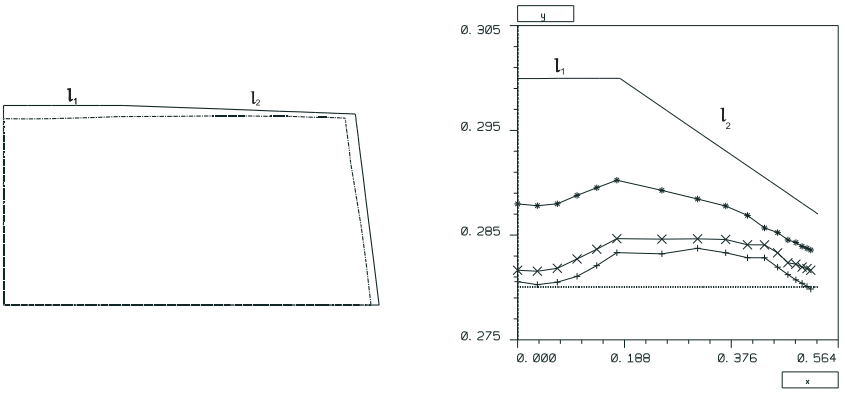

Fig. 19 Contraction in a cross-section about half-way up the slab; l_1, l_2 label two of the three-segments of the inner face of the moulding collar. Numerical cross-sectional profile of the wide side at three different heights ($+-$ lower region, $\times-$ halfway region, $*-$ head region, $-$ mould geometry, $\cdots$ desired geometry) are shown in the graphic on the right.

5.2 Numerical results for the two-dimensional simulation of the start stage

When using the SBM algorithm, the computational cost of the start stage simulation made difficult the real-time usage of this method to help in the understanding of the different effects in the casting process. Due to this, we have restricted ourselves to the two-dimensional case in the symmetry plane $x_1 = 0$, and we have developed two new algorithms, NBM and VNBM, which were presented in Section 4, to improve and to accelerate the real-time response for the butt curl simulation; in this section we compare the efficiency between the three algorithms when they are applied to simulate it.

The parameters considered to carry out the aluminium alloy casting simulations are the following:

– for the SBM algorithm:

$$\gamma_c = 0.5e6,\ \lambda_c = 1.e{-}6,\ \gamma_p = 1.25e{-}12,\ \lambda_p = 0.4e12,\ \vartheta = 0.9;$$

– for the NBM algorithm:

$$\lambda_c = 1,\ \epsilon_c = 1.e{-}3,\ \lambda_p = 1,\ \vartheta = 0.9;$$

– for the VNBM algorithm:

$$\lambda_c = 1,\ \epsilon_c = 1.e{-}3,\ \gamma_p^0 = 1.25e{-}13,\ \vartheta = 0.9.$$

Figure 20 shows the mesh of the computational domain at the start of the casting process with 1320 elements and 732 nodes. In this mesh, we took into account the peculiarities of casting processes, and in its numbering, the first nodes correspond with the contact ones to use the partial factorization technique shown in Subsection 4.3.1.

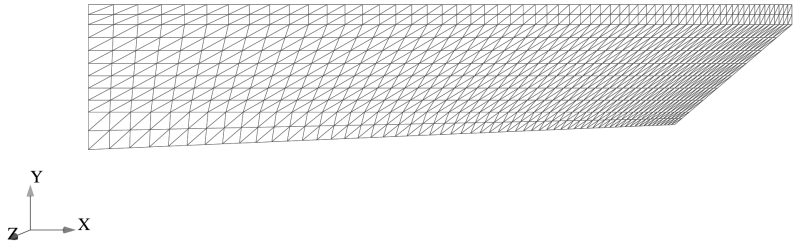

Fig. 20 Initial mesh of the slab used for the start stage.

The considered time interval is $(0, 145\text{s}]$ and an initial time step $\Delta t = 1\text{s}$ is used. Since butt curl is so rapid (see Figure 17, on right), its accurate modelling requires time steps to be small, so, to obtain a good initial approach which is necessary in the Newton algorithm, the NBM algorithm incorporates the time step optimization explained in Subsection 4.3.4.

Figure 21 shows the isotherms obtained with the code developed in Otero [70] after carry out a physical parameters adjustment with experimental data, and the butt curl obtained at the last time step.

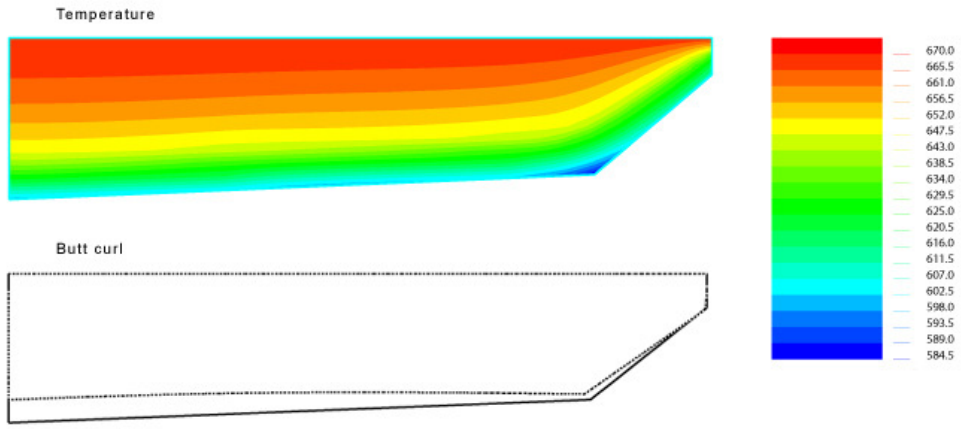

Fig. 21 Isotherms and butt curl deformation after 145s of casting.

The numerical simulation was carried out by using the three algorithms. Although the NBM algorithm had a very good convergence in academic problems (see [5]), in this real casting simulation, convergence is not always achieved, mainly when a zone of the slab is recently solidified. Besides, the SBM algorithm has a good but slow convergence which dependes strongly on the

chosen parameters. Fortunately, the VNBM algorithm incorporates the good convergence properties of the Newton algorithm in contact and it improves the convergence of the fixed point algorithm in viscoplasticity with the automatic computation of the algorithm parameters.

The cpu-time and the average number of iterations obtained with the SBM and VNBM algorithms are summarized in Table 11. Data for the NBM algorithm are not shown since, as we have said, convergence is not always achieved.

Table 11 Cpu-time and number of iterations after $145s$ of casting.

Method	SBM	VNBM
cpu-time (s)	2660.49	465.562
iterations	6593	89

Notice that with the VNBM algorithm the cpu-time decreases approximately 83% with respect to the SBM algorithm and the number of iterations decreases 99%.

6 Conclusions

In this work we have collected three algorithms to solve numerically a Signorini contact problem in Maxwell-Norton materials arising from aluminium alloys casting processes. Along all the paper we have analyzed the efficiency of these algorithms not only on academic tests but also to simulate casting processes.

In [3], Barral presented a numerical method based on the Bermúdez-Moreno algorithm involving two multipliers which can be obtained as fixed points of two nonlinear equations. Due to the slow convergence of this algorithm and its strong dependence on the parameters, we have reviewed two techniques to improve its efficiency: firstly, taking advantage of the good convergence properties of Newton methods and secondly, by means of considering the parameters of the Bermúdez-Moreno algorithm as variable scalar functions. Numerical results show that:

- The standard Bermúdez-Moreno algorithm (SBM) is slower but in turn very robust.
- The Newton algorithm combined with some numerical strategies (NBM algorithm) is faster and more accurate. It needs fewer iterations and less cpu-time than the SBM one. The numerical strategies presented in this paper –the matrix factorization adapted to the problem geometry, an adimensionalization technique and a time step optimization– work very well in academic examples. Nevertheless, convergence is not always achieved when they are applied to the casting simulation. Our guess is that this unexpected difficulty is due to the very different behaviours found in casting processes (between recently solidified zones and others already cold).

– The main disadvantage of the SBM algorithm is its strong dependence on the parameters (see [7]). The Bermúdez-Moreno algorithm with variable parameters for viscoplasticity combined with the Newton method for contact (VNBM algorithm) overcomes this difficulty since the viscoplastic parameters are considered variable scalar functions, depending on time and space and they are automatically calculated. Moreover, it takes advantage of the good convergence properties of Newton method when solving the nonlinear contact condition. Numerical results in casting simulations show that the VNBM algorithm is the best option to simulate the butt curl deformation.

Acknowledgements This work was supported by Spanish Ministry of Education and Culture (projects MAT96-0715, DPI2001-2908), Spanish Ministry of Education and Science (project DPI2004-01993), Spanish Ministry of Science and Innovation (project MTM2008-05682) and Spanish Ministry of Economy and Competitiveness (project MTM2011-23976), by Xunta de Galicia (projects PGIDT00PXI20701PR, PGIDT02XI20701PN and INCITE09 207 093 PR) and by ALCOA-INESPAL, A Coruña, Spain, under contract.

References

1. Agelet de Saracibar, C., Chiumenti, M., Cervera, M.: Current developments on the coupled thermomechanical computational modeling of metal casting processes. Comput. Meth. Mater. Sci. **6**, 15–25 (2006)
2. Arregui, I., Cendán, J.J., Parés, C., Vázquez, C.: Numerical solution of a 1-D elastohydrodynamic problem in magnetic storage devices. ESAIM: Math. Model. Numer. Anal. **42**, 645–665 (2008)
3. Barral, P.: Análisis matemático y simulación numérica del comportamiento termomecánico de una colada de aluminio. Ph.D. thesis, Universidade de Santiago de Compostela, Spain (2001)
4. Barral, P., Bermúdez, A., Muñiz, M.C., Otero, M.V., Quintela, P., Salgado, P.: Numerical simulation of some problems related to aluminium casting. J. Mater. Process. Technol. **142**(2), 383–399 (2003)
5. Barral, P., Moreno, C., Quintela, P., Sánchez, M.T.: A numerical algorithm for a Signorini problem associated with Maxwell-Norton materials by using generalized Newton's methods. Comput. Methods Appl. Mech. Engrg. **195**(9-12), 880–904 (2006)
6. Barral, P., Naya-Riveiro, M.C., Quintela, P.: Mathematical analysis of a viscoelastic problem with temperature-dependent coefficients. I. Existence and uniqueness. Math. Methods Appl. Sci. **30**(13), 1545–1568 (2007)
7. Barral, P., Quintela, P.: A numerical method for simulation of thermal stresses during casting of aluminium slabs. Comput. Methods Appl. Mech. Engrg. **178**(1-2), 69–88 (1999)
8. Barral, P., Quintela, P.: A numerical algorithm for prediction of thermomechanical deformation during the casting of aluminium alloy ingots. Finite Elem. Anal. Des. **34**(2), 125–143 (2000)
9. Barral, P., Quintela, P.: Numerical analysis of a viscoplastic problem with contact condition taking place in an aluminium casting. J. Comput. Appl. Math. **115**(1-2), 63–86 (2000)
10. Barral, P., Quintela, P.: Asymptotic justification of the treatment of a metallostatic pressure type boundary condition in an aluminium casting. Math. Models Methods Appl. Sci. **11**(6), 951–977 (2001)
11. Barral, P., Quintela, P.: Asymptotic analysis of a metallostatic pressure type boundary condition modelled by a fictitious domain method in an aluminium casting. Asymptot. Anal. **30**(2), 93–116 (2002)

12. Barral, P., Quintela, P.: Existence of a solution for a Signorini contact problem for Maxwell-Norton materials. IMA J. Appl. Math. **67**(6), 525–549 (2002)
13. Barral, P., Quintela, P., Sánchez, M.T.: Newton's algorithm combined with factorization strategies for nonlinear problems arising from industrial processes. In: Coupled Problems 2005. An Eccomas Thematic Conference, Abstracts CD (2005)
14. Barral, P., Quintela, P., Sánchez, M.T.: A Bermúdez-Moreno algorithm adapted to solve a viscoplastic problem in alloy solidification processes. Accepted for publication in ESAIM-Math. Model. Numer. Anal. (2013)
15. Barral, P., Sánchez, M.T.: A suitable numerical algorithm for the simulation of the butt curl deformation of an aluminium slab. In: Numerical mathematics and advanced applications, pp. 1108–1116. Springer, Berlin (2006)
16. Bellet, M., Jaouen, O., Poitrault, I.: An ALE-FEM approach to the thermomechanics of solidification processes with application to the prediction of pipe shrinkage. Int. J. Numer. Methods Heat Fluid Flow **15**(2), 120–142 (2005)
17. Bensoussan, A., Frehse, J.: Asymptotic behaviour of the time dependent Norton-Hoff law in plasticity theory and H^1 regularity. Comment. Math. Univ. Carolinae **37**, 285–304 (1996)
18. Bermúdez, A., Gómez, D., Muñiz, M.C., Salgado, P.: Transient numerical simulation of a thermoelectrical problem in cylindrical induction heating furnaces. Adv. Comput. Math. **26**(1-3), 39–62 (2007)
19. Bermúdez, A., Moreno, C.: Duality methods for solving variational inequalities. Comput. Math. Appl. **7**(1), 43–58 (1981)
20. Bermúdez, A., Muñiz, M.C.: Numerical solution of a free boundary problem taking place in an electromagnetic casting. Math. Models Methods Appl. Sci. **9**(9), 1393–1416 (1999)
21. Bermúdez, A., Muñiz, M.C., Salgado, P.: Asymptotic approximation and numerical simulation of electromagnetic casting. Metall. Mater. Trans. B **34B**(1), 83–91 (2003)
22. Bermúdez, A., Nogueiras, M.R., Vázquez, C.: Numerical solution of variational inequalities for pricing Asian options by higher order Lagrange-Galerkin methods. Appl. Numer. Math. **56**(10-11), 1256–1270 (2006)
23. Bermúdez, A., Otero, M.V.: Numerical solution of a three-dimensional solidification problem in aluminium casting. Finite Elem. Anal. Des. **40**(13-14), 1885–1906 (2004)
24. Bertsekas, D.P.: Nonlinear Programming. Athena Scientific, Belmont (1995)
25. Besson, O., Bourgeois, J., Chevalier, P.A., Rappaz, J., Touzani, R.: Numerical modelling of electromagnetic casting processes. J. Comput. Phys. **92**, 482–507 (1991)
26. Blanchard, D., Le Tallec, P.: Numerical analysis of the equations of small strains quasistatic elastoviscoplasticity. Numer. Math. **50**(2), 147–169 (1986)
27. Bower, A.F.: Applied Mechanics of Solids. CRC Press (2010)
28. Burguera, M., Viaño, J.M.: Numerical solving of frictionless contact problems in perfectly plastic bodies. Comput. Methods Appl. Mech. Engrg. **121**(1-4), 303–322 (1995)
29. Casella, E., Giangi, M.: An analitical and numerical study of the stefan problem with convection by means of an entalphy method. Math. Methods Appl. Sci. **24**(9), 623–639 (2001)
30. Cervera, M., Agelet de Saracibar, C., Chiumenti, M.: Thermo-mechanical analysis of industrial solidification processes. Int. J. Num. Meths. Engng. **46**, 1575–1591 (1999)
31. Chen, Z., Jiang, L.: Approximation of a two-phase continuous casting Stefan problem. J. Partial Differential Equations **11**, 59–72 (1998)
32. Chen, Z., Shih, T., Yue, X.: Numerical methods for Stefan problems with prescribed convection and nonlinear flux. IMA J. Numer. Anal. **20**(1), 81–98 (2000)
33. Ciarlet, P.G.: Élasticité tridimensionnelle, *Recherches en Mathématiques Appliquées [Research in Applied Mathematics]*, vol. 1. Masson, Paris (1986)
34. Ciavaldini, J.R.: Analyse numérique d'un probléme de Stefan á deux phases par une methode d'elements finis. SIAM J. Numer. Anal. **2**, 464–487 (1975)
35. Djaoua, M., Suquet, P.: Évolution quasi-statique des milieux visco-plastiques de Maxwell-Norton. Math. Methods Appl. Sci. **6**(2), 192–205 (1984)
36. Domitner, J., Drezet, J.M., Wu, M., Ludwig, A.: Thermo-mechanical modeling of dendrite deformation in continuous casting of steel. IOP Conference Series: Materials Science and Engineering **33**(1), 012,058 (2012)

37. Drezet, J., Rappaz, M., Krahenbuhl, Y.: Thermomechanical effects during direct chill and electromagnetic casting of aluminum alloys. Part II: numerical simulation. Light Metals pp. 941–950 (1995)
38. Drezet, J.M., Plata, M.: Thermomechanical effects during direct chill and electromagnetic casting of aluminum alloys. Part I: Experimental investigation. Light Metals pp. 931–940 (1995)
39. Durany, J.: Contribución al estudio matemático del problema de Stefan en medios no homogéneos. Ph.D. thesis, Universidade de Santiago de Compostela, Spain (1983)
40. El-Raghy, T.S., El-Demerdash, H.A., Ahmed, H.A., El-Sheikh, A.M.: Modelling of the transient and steady state periods during aluminium DC casting. Light Models pp. 925–929 (1995)
41. Facchinei, F., Pang, J.S.: Finite-dimensional variational inequalities and complementarity problems. Springer Series in Operations Research. Springer-Verlag, New York (2003)
42. Flemings, M.C.: Solidification processing. In: McGraw-Hill Series in Materials Science and Engineering. McGraw-Hill, New York (1974)
43. Friaâ, A.: Le matériau de Norton-Hoff généralisé et ses applications en analyse limite. C. R. Acad. Sci. Paris Sér. A-B **286**(20), A953–A956 (1978)
44. Friaâ, A.: La loi de Norton-Hoff généralisée en plasticité et viscoplasticité. Ph.D. thesis, Universite Pierre et Marie Curie, Paris (1979)
45. Gallardo, J.M., Parés, C., Castro, M.: A generalized duality method for solving variational inequalities. Applications to some nonlinear Dirichlet problems. Numer. Math. **100**(2), 259–291 (2005)
46. Geymonat, G., Suquet, P.: Functional spaces for Norton-Hoff materials. Math. Methods Appl. Sci. **8**(2), 206–222 (1986)
47. Glowinski, R., Le Tallec, P.: Augmented Lagrangian and operator-splitting methods in nonlinear mechanics, *SIAM Studies in Applied Mathematics*, vol. 9. Society for Industrial and Applied Mathematics (SIAM), Philadelphia, PA (1989)
48. Gurtin, M.E.: An introduction to continuum mechanics, *Mathematics in Science and Engineering*, vol. 158. Academic Press Inc. [Harcourt Brace Jovanovich Publishers], New York (1981)
49. Gurtin, M.E., Fried, E., Anand, L.: The Mechanics and Thermodynamics of Continua. Cambridge University Press, New York (2010)
50. Hannart, B., Cialti, F., Schalkwijk, R.: Thermal stresses in DC casting of aluminium slabs: Application of a finite element model. Light Metals pp. 879–887 (1994)
51. Hatch, J.E.: Aluminum: Properties and Physical Metallurgy. American Society for Metals, Ohio (2005)
52. Hill, R.: The Mathematical Theory of Plasticity. Oxford, at the Clarendon Press (1950)
53. Hongjun, H., Dingfei, Z., MingBo, Y.: Numerical simulation of thermal stress in cast billets made of AZ31 magnesium alloy during direct-chill casting. J. Manuf. Process. **10**, 82–88 (2008)
54. Kaufman, J.G., Rooy, E.L.: Aluminum Alloy Castings. Properties, Processes, and Applications. ASM International, Ohio (2004)
55. Kikuchi, N., Oden, J.T.: Contact problems in elasticity: a study of variational inequalities and finite element methods, *SIAM Studies in Applied Mathematics*, vol. 8. Society for Industrial and Applied Mathematics (SIAM), Philadelphia, PA (1988)
56. Kim, K.Y.: Analysis of Gap Formation at Mold-Shell Interface during Solidification of aluminium Alloy Plate. ISIJ International **43**(5), 647–652 (2003)
57. Kinderlehrer, D., Stampacchia, G.: An introduction to variational inequalities and their applications. Pure and Applied Mathematics. Academic Press, New York (1980)
58. Kristiansson, J.O., Zetterlund, E.H.: Thermal Stresses and Strains in the Solidifying Shell Within the Primary Cooling Zone During Continuous Casting. In: Numerical Methods in Industrial Forming Processes, pp. 413–423. Pineridge Press limited, Swansea, United Kingdom (1982)
59. Le, Q., Guo, S., Zhao, Z., Cui, J., Zhang, X.: Numerical simulation of electromagnetic DC casting of magnesium alloys. J. Manuf. Process. **183**, 194–201 (2007)
60. Le Tallec, P.: Numerical analysis of viscoelastic problems. Recherches en Mathémathiques Appliquées. Masson, Paris (1990)

61. Lemaitre, J., Chaboche, J.L.: Mécanique des matériaux solides. Dunod, Paris (1988)
62. Lewis, R.W., Ravindran, K.: Finite element simulation of metal casting. Int. J. Numer. Meth. Eng. **47**, 29–659 (2000)
63. Morales de Luna, T., Castro Díaz, M.J., Parés Madroñal, C.: A duality method for sediment transport based on a modified Meyer-Peter & Müller model. J. Sci. Comput. **48**(1-3), 258–273 (2011)
64. Mariaux, S., Rappaz, M., Krahenbuhl, Y., Plata, M.: Modelling of Thermomechanical Effects During the Start-Up Phase of the Electromagnetic Casting Process. In: Advances in Production and Fabrication of Light Metals and Metal Matrix Composites, pp. 175–187. Canadian Inst. of Mining, Metallurgy and Petroleum, Montreal, Canada (1992)
65. Marsden, J.E., Hughes, T.J.R.: Mathematical Foundations of Elasticity. Prentice-Hall, New Jersey (1983)
66. Meirmanov, A.M.: The Stefan problem. Walter de Gruyter, New York (1992)
67. Murat, M.: Compacité par compensation. Ann. Scuola Norm. Sup. Pisa Cl. Sci. (4) **5**, 489–507 (1978)
68. Naya-Riveiro, M.C., Quintela, P.: Modelling of materials with long memory. Int. J. Solids Struct. **45**(24), 1755–1768 (2008)
69. Nedjar, B.: An entalphy-based finite element method for nonlinear heat problems involving phase change. Comput. Struct. **80**(1), 9–21 (2002)
70. Otero, M.V.: Estudio matemático y resolución numérica de modelos que surgen en el estudio de una colada de aluminio. Ph.D. thesis, Universidade de Santiago de Compostela, Spain (2004)
71. Özisik, M.N.: Boundary value problems of heat conduction. Dover Publications Inc., New York (1989)
72. Pang, J.S.: A B-differentiable equation-based, globally and locally quadratically convergent algorithm for nonlinear programs, complementarity and variational inequality problems. Math. Programming **51**(1, (Ser. A)), 101–131 (1991)
73. Parés, C., Castro, M., Macías, J.: On the convergence of the Bermúdez-Moreno algorithm with constant parameters. Numer. Math. **92**(1), 113–128 (2002)
74. Parés, C., Macías, J., Castro, M.: Duality methods with an automatic choice of parameters. Application to shallow water equations in conservative form. Numer. Math. **89**(1), 161–189 (2001)
75. Robinson, S.M.: Newton's method for a class of nonsmooth functions. Set-Valued Anal. **2**(1-2), 291–305 (1994)
76. Rubinstein, L.I.: The Stefan problem. No. 27 in Translations of Mathematical Monographs. American Mathematical Society, Providence, R.I. (1971)
77. Sánchez, M.T.: Mathematical Analysis and Numerical Simulation of some nonlinear problems in solid mechanics. Ph.D. thesis, Universidade de Santiago de Compostelas, Spain (2009)
78. Schneider, W., Jensen, E.K., Carrupt, B.: Development of a new starting block shape for the dc casting of sheet ingots. Part I: Experimental results. Light Metals pp. 961–967 (1995)
79. Sołek, K., Trębacz, L.: Thermo-Mechanical Model of Steel Continuous Casting Process. Arch. Metall. Mater. **57**(1), 355–361 (2012)
80. Stefanescu, D.M.V.C.: ASM Handbook. Casting, vol. 15. ASM International. The Materials Information Society, Ohio (1992)
81. Stoll, H.W.: Casting Design Issues and Practices. Casting Design and Performance. ASM International. The Materials Information Society, Ohio (2009)
82. Subroto, T., Miroux, A., Mortensen, D., M'Hamdi, M., Eskin, D.G., Katgerman, L.: Semi-quantitative predictions of hot tearing and cold cracking in aluminum dc casting using numerical process simulator. IOP Conference Series: Materials Science and Engineering **33**(1), 012,068 (2012)
83. Sullivan, J.M., Lynch, D.R.: Numerical simulation of dendritic solidification of an undercooled melt. Int. J. Numer. Meth. Engng. **25**, 415–444 (1988)
84. Temam, R.: Problèmes Mathématiques en Plasticité. Méthodes Mathématiques de l'Informatique. Gauthier-Villars, Paris (1983)
85. Wong, W.A., Jonas, J.J.: Aluminum extrusion as a thermally activated process. Trans. Metall. Soc. AIME **242**, 2271–2280 (1968)

86. Wriggers, P.: Finite element algorithms for contact problems. Arch. Comput. Methods Engrg. **2**(4), 1–49 (1995)
87. Wu, Y., Hill, J.M., Flint, P.J.: A novel finite element method for heat transfer in the continuous caster. J. Aust. Math. Soc. B **35**(3), 263–288 (1994)
88. Xu, Y., Wang, J.C., Guo, S.J., Li, X.T., Xue, G.X.: Effects of water-restricted panel on the casting process of high strength aluminum alloy ingots. J. Manuf. Process. **211**, 78–83 (2011)
89. Yoo, J., Rubinsky, B.: Numerical computation using finite elements for the moving interface in heat transfer problems with phase transformation. Numer. Heat Tranf. **6**, 209–222 (1983)
90. Yoo, J., Rubinsky, B.: A finite element method for the study of solidification processes in the presence of natural convection. Int. J. Numer. Meth. Engng **23**, 1785–1805 (1986)